of the yeast-based procedure for GPCR mutagenesis has been proven.

Human formyl peptide receptor like-1, which was originally identified as an orphan GPCR, has been used to isolate agonists for GPCRs of unknown function [77]. Histidine prototrophic selection by the *FUS1–HIS3* reporter gene was performed with secreted random tridecapeptides as a library and a mammalian/yeast hybrid Gα subunit which allows functional coupling with the receptor. As a result, surrogate agonists as peptidic candidates have been successfully screened, and the promoted activation of formyl peptide receptor like-1 expressed in human cells has been validated with synthetic versions of the peptides.

Pheromone signaling-based screening systems – protein–protein interactions

Yeast–mammal chimeric Gα system

Medici *et al.* [78] constructed an intelligent system for analysis of protein–protein interactions by managing heterotrimeric G-protein signaling in yeast (Fig. 3A). They initially found that a fusion protein between the yeast Ste2p receptor lacking the last 62 amino acids of the cytoplasmic tail and the full-length Gpa1p transduced the signal in response to the binding of α-factor in cells devoid of both endogenous *STE2* and endogenous *GPA1*. Subsequently, a yeast–mammal chimeric Gα composed of the N-terminal 362 amino acids of Gpa1p and the C-terminal 128 amino acids of rat $G\alpha_s$ was prepared. The chimeric Gα is able to interact with the yeast Gβγ complex, but is not able to interact with the yeast Ste2p receptor, and it was fused to the truncated Ste2p receptor. Although a *gpa1*Δ yeast strain harboring the yeast–rat chimeric Gα does not respond to pheromone, a *ste2*Δ *gpa1*Δ yeast strain expressing the Ste2p–Gpa1p–$G\alpha_s$ fusion protein that is covalently linked to Ste2p and the chimeric Gα displayed a strong pheromone response in the presence of α-factor. These results suggest that the specific interaction of the receptor with the C-terminus of Gα is necessary to bring the two proteins into close proximity. This hypothesis was applied to the analysis of protein–protein interactions. It was demonstrated that the interaction of Gpa1p–$G\alpha_s$ fused to protein X and Ste2p receptor fused to protein Y permitted pheromone response signaling through the contact between Ste2p and Gpa1p–$G\alpha_s$, using the interaction between Snf1 and Snf4, which form a kinase complex regulating transcriptional activation in glucose derepression, or between Raf and the constitutively active form of Ras (Table 1). In this system, a *gpa1*Δ haploid strain harboring the plasmid, which complements Gpa1p function to capture Ste4p/Ste18p subunits, or a *GPA1/gpa1*Δ diploid yeast strain was used to avoid lethality by spontaneous signaling from the liberated Ste4p/Ste18p subunits.

Gγ interfering system

The Gγ interfering system (it was called a G-protein fusion system in the original literature) has been developed to monitor integral membrane protein–protein interactions and to screen for negative mutants with loss of the interaction capacity (Fig. 3B) [79]. The yeast Gγ-subunit Ste18p was genetically fused to the C-terminus of cytoplasmic protein X, and the protein X–Gγ fusion protein and integral membrane protein Y in its native form were coexpressed in a *ste18*Δ strain. The interaction between protein X–Gγ and protein Y inhibits pheromone signaling through the Gβγ complex, in spite of the presence of α-factor, whereas a lack of interaction between protein X and protein Y normally leads to signaling. This event might be attributed to the fact that restrictive localization or structural interruption by trapping of the Gβγ complex at the position of protein Y on the membrane disturbs the contact with its subsequent effector. In one example, interactions of attractive drug target candidates, syntaxin 1a and nSec1 or fibroblast-derived growth factor receptor 3 and SNT-1, were monitored, and nSec1 mutants that lost the ability to bind to syntaxin 1a were successfully identified by taking advantage of growth arrest induced through the protein–protein interaction [79] (Table 1).

Gγ recruitment system

The above-described systems for analysis of protein–protein interactions using pheromone signaling are proven techniques for selecting target proteins involved with membrane proteins. However, they might generate relatively high background signals, making them unfavorable for screening candidates by growth selection, because the machinery for distinguishing interactions does not always ensure complete inactivation of signaling in the presence of pheromone.

The Gγ recruitment system has recently been developed using the pheromone signaling pathway, and is a dependable system that completely eliminates background signals for noninteracting protein pairs in the presence of pheromone (Fig. 3C) [80]. This system can be used to investigate cytosolic–cytosolic or cytosolic–membrane protein interactions. A yeast strain with a mutated Gγ lacking membrane localization ability

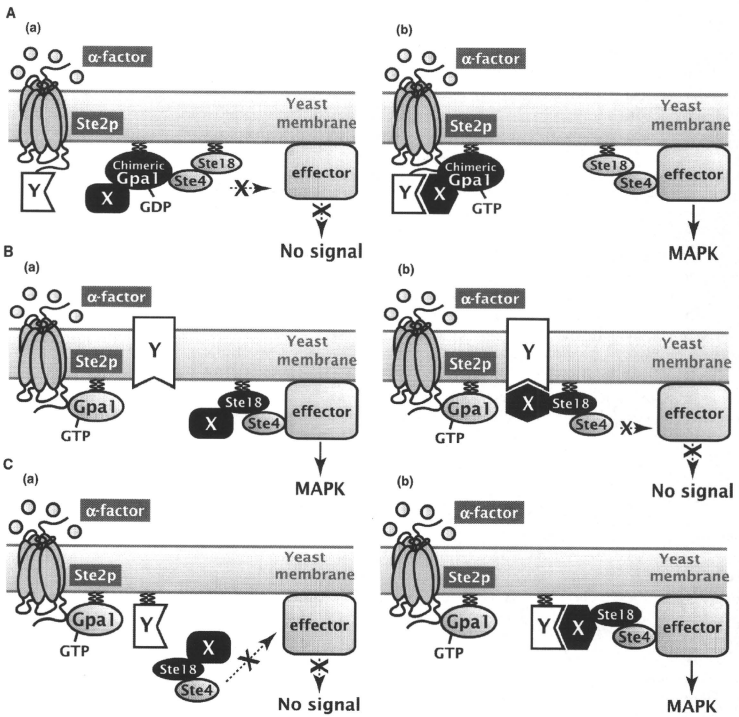

Fig. 3. Schematic illustration of pheromone signaling-based screening systems for protein–protein interaction analysis. (A) The yeast–mammal chimeric Gα system uses chimeric Gpa1p, which is able to interact with the yeast Gβγ complex, but not with the yeast Ste2p receptor. Chimeric Gpa1p is fused to protein X, and yeast Ste2p receptor is fused to protein Y. (a) Noninteracting protein pairs are unable to activate the pheromone signaling pathway. (b) Interacting protein pairs bring Ste2p and chimeric Gpa1p into close proximity, and permit physical contact between the two, resulting in activation of pheromone signaling. (B) The Gγ interfering system can screen for negative mutants that do not interact. Ste18p genetically fused to the C-terminus of cytoplasmic protein X and integral membrane protein Y are coexpressed in a *ste18Δ* strain. (a) Noninteracting protein pairs are able to activate the pheromone signaling pathway. (b) Interacting protein pairs are unable to activate the pheromone signaling pathway, owing to the interruption of contacts between the Gβγ complex and its effector. (C) The Gγ recruitment system can completely eliminate background signals for noninteracting protein pairs. Mutated Ste18p lacking membrane localization fused to cytoplasmic protein X and membrane-associated protein Y are coexpressed in a *ste18Δ* strain. (a) Noninteracting protein pairs completely lack pheromone signaling, owing to the release of the Ste4p–Ste18p complex into the cytosol. (b) Interacting protein pairs restore signaling, owing to the recruitment of the Gβγ complex onto the plasma membrane.

($G\gamma_{cyto}$) should be prepared by deletion of the dual lipid modification sites in the C-terminus of Ste18p, because yeast pheromone signaling strictly requires the localization of the Gβγ complex to the plasma membrane [41,42]. The release of Ste18p into the cytosol eliminates the signaling ability mediated by the Ste4p–Ste18p complex [41], and this technique therefore leads to absolute interruption of background

signals. One test protein must be soluble and fused with $G\gamma_{cyto}$ to be expressed in the cytosol but not the membrane, whereas the other may be soluble but should have an added lipid modification site to allow association with the inner leaflet of plasma membrane, or it may be an intrinsically hydrophobic integral membrane protein or lipidated element of a membrane-associated protein. Consequently, when the cytosolic protein X–$G\gamma_{cyto}$ fusion protein and the membrane-associated protein Y are expressed in a *ste18*Δ haploid strain in the presence of α-factor pheromone, the interaction between protein X and protein Y restores signaling, owing to the recruitment of the Gβγ complex onto the plasma membrane, which can be monitored, but a lack of interaction between protein X and protein Y results in no background signaling.

In an original report, the ZZ domain derived from protein A of *Staphylococcus aureus* and the Fc portion of human IgG, which are both soluble proteins, were used as a model interaction pair (Table 1). The ZZ domain is a tandemly repeated Z domain that binds to human Fc protein and displays higher affinity than a Z domain monomer [81]. The interaction between the ZZ domain with an attached dual lipidation motif in its C-terminus and Fc fused to the C-terminus of $G\gamma_{cyto}$ was easily detected with a transcriptional assay using the pheromone response *FIG1* promoter and a *GFP* reporter gene or a halo bioassay by growth arrest, whereas background signals from noninteracting pairs were never observed, owing to the loss of localization of the yeast Gβγ complex at the plasma membrane.

The wild-type and two variants of the Z domain that each possess a single mutation and exhibit different affinity constants were expressed as additional interaction pairs for the Fc fusion protein [82]. All variants with a wide range of affinity constants, from 8.0×10^3 to 6.8×10^8 M^{-1} [83], were clearly detectable, and moreover, the relatively faint interaction with an affinity constant of 8.0×10^3 M^{-1} was successfully detected because of the complete elimination of background signal for noninteracting pairs (Table 1). Surprisingly, a logarithmic proportional relationship between affinity constants and fluorescence intensities measured by the transcriptional assay was observed, suggesting that this approach may facilitate the rapid assessment of affinity constants.

Finally, the Gγ recruitment system has more recently been improved by the expression of a third cytosolic protein that competes with the candidate protein [102]. The competitor-introduced Gγ recruitment system could specifically isolate only affinity-enhanced variants from libraries containing a large majority of original proteins, clearly indicating the applicability of this new approach to directed evolution.

Concluding remarks

Yeast-based approaches with the G-protein signaling machineries presented here are remarkably useful for the detection and screening of interactions of proteins involved in various biological processes. These systems are essentially comparable to the Y2H systems that have been predominantly used to screen protein–protein interaction partners from large-scale libraries and to estimate the relative strengths of interactions, but are additionally able to detect activation or inactivation associated with the switching machinery of signaling molecules, such as major pharmaceutical targets of GPCRs. Yeast-based and signaling-mediated screening systems are obviously powerful and practical tools with which to quickly screen for possible candidates. In the future, we can be sure that they will be improved, with more powerful and user-friendly advanced modifications, and will be widely applied to various fields, such as protein engineering.

Acknowledgements

This work was supported in part by a Research Fellowship for Young Scientists from the Japan Society for the Promotion of Science and a Special Coordination Fund for Promoting Science and Technology, Creation of Innovation Centers for Advanced Interdisciplinary Research Areas (Innovative Bioproduction Kobe), from the Ministry of Education, Culture, Sports, Science and Technology (MEXT), Japan.

References

1 Sychrová H (2004) Yeast as a model organism to study transport and homeostasis of alkali metal cations. *Physiol Res* **53**, S91–S98.
2 Lushchak VI (2006) Budding yeast *Saccharomyces cerevisiae* as a model to study oxidative modification of proteins in eukaryotes. *Acta Biochim Pol* **53**, 679–684.
3 Wang Y & Dohlman HG (2006) Regulation of G protein and mitogen-activated protein kinase signalling by ubiquitination: insights from model organisms. *Circ Res* **99**, 1305–1314.
4 Schneiter R (2007) Intracellular sterol transport in eukaryotes, a connection to mitochondrial function? *Biochimie* **89**, 255–259.
5 Winderickx J, Delay C, De Vos A, Klinger H, Pellens K, Vanhelmont T, Van Leuven F & Zabrocki P (2008) Protein folding diseases and neurodegeneration: lessons

learned from yeast. *Biochim Biophys Acta* **1783**, 1381–1395.

6 Fields S & Song O (1989) A novel genetic system to detect protein–protein interactions. *Nature* **340**, 245–246.

7 Gyuris J, Golemis E, Chertkov H & Brent R (1993) Cdi1, a human G1 and S phase protein phosphatase that associates with Cdk2. *Cell* **75**, 791–803.

8 SenGupta DJ, Zhang B, Kraemer B, Pochart P, Fields S & Wickens M (1996) A three-hybrid system to detect RNA–protein interactions *in vivo*. *Proc Natl Acad Sci USA* **93**, 8496–8501.

9 Vidal M, Brachmann RK, Fattaey A, Harlow E & Boeke JD (1996) Reverse two-hybrid and one-hybrid systems to detect dissociation of protein–protein and DNA–protein interactions. *Proc Natl Acad Sci USA* **93**, 10315–10320.

10 Marsolier MC, Prioleau MN & Sentenac A (1997) A RNA polymerase III-based two-hybrid system to study RNA polymerase II transcriptional regulators. *J Mol Biol* **268**, 243–249.

11 Stagljar I, Korostensky C, Johnsson N & Heesen ST (1998) A genetic system based on split-ubiquitin for the analysis of interactions between membrane proteins *in vivo*. *Proc Natl Acad Sci USA* **95**, 5187–5192.

12 Möckli N, Deplazes A, Hassa PO, Zhang Z, Peter M, Hottiger MO, Stagljar I & Auerbach D (2007) Yeast split-ubiquitin-based cytosolic screening system to detect interactions between transcriptionally active proteins. *BioTechniques* **42**, 725–730.

13 Urech DM, Lichtlen P & Barberis A (2003) Cell growth selection system to detect extracellular and transmembrane protein interactions. *Biochim Biophys Acta* **1622**, 117–127.

14 Chen J, Zhou J, Sanders CK, Nolan JP & Cai H (2009) A surface display yeast two-hybrid screening system for high-throughput protein interactome mapping. *Anal Biochem* **390**, 29–37.

15 Uetz P, Giot L, Cagney G, Mansfield TA, Judson RS, Knight JR, Lockshon D, Narayan V, Srinivasan M, Pochart P *et al.* (2000) A comprehensive analysis of protein–protein interactions in *Saccharomyces cerevisiae*. *Nature* **403**, 623–627.

16 Ito T, Chiba T, Ozawa R, Yoshida M, Hattori M & Sakaki Y (2001) A comprehensive two-hybrid analysis to explore the yeast protein interactome. *Proc Natl Acad Sci USA* **98**, 4569–4574.

17 Stelzl U, Worm U, Lalowski M, Haenig C, Brembeck FH, Goehler H, Stroedicke M, Zenkner M, Schoenherr A, Koeppen S *et al.* (2005) A human protein–protein interaction network: a resource for annotating the proteome. *Cell* **122**, 957–968.

18 Rual JF, Venkatesan K, Hao T, Hirozane-Kishikawa T, Dricot A, Li N, Berriz GF, Gibbons FD, Dreze M, Ayivi-Guedehoussou N *et al.* (2005) Towards a proteome-scale map of the human protein–protein interaction network. *Nature* **437**, 1173–1178.

19 Paravicini G & Friedli L (1996) Protein–protein interactions in the yeast *PKC1* pathway: Pkc1p interacts with a component of the MAP kinase cascade. *Mol Gen Genet* **251**, 682–691.

20 Sawka-Verhelle D, Filloux C, Tartare-Deckert S, Mothe I & Van Obberghen E (1997) Identification of Stat 5B as a substrate of the insulin receptor. *Eur J Biochem* **250**, 411–417.

21 Wu W, Niles EG, Hirai H & LoVerde PT (2007) Identification and characterization of a nuclear receptor subfamily I member in the Platyhelminth *Schistosoma mansoni* (SmNR1). *FEBS J* **274**, 390–405.

22 Thaminy S, Auerbach D, Arnoldo A & Stagljar I (2003) Identification of novel ErbB3-interacting factors using the split-ubiquitin membrane yeast two-hybrid system. *Genome Res* **13**, 1744–1753.

23 Camus C, Geymonat M, Garreau H, Baudet-Nessler S & Jacquet M (1997) Dimerization of Cdc25p, the guanine-nucleotide exchange factor for Ras from *Saccharomyces cerevisiae*, and its interaction with Sdc25p. *Eur J Biochem* **247**, 703–708.

24 Li Y, Wei K, Lu C, Li Y, Li M, Xing G, Wei H, Wang Q, Chen J, Wu C *et al.* (2002) Identification of hepatopoietin dimerization, its interacting regions and alternative splicing of its transcription. *Eur J Biochem* **269**, 3888–3893.

25 Lezzi M, Bergman T, Henrich VC, Vögtli M, Frömel C, Grebe M, Przibilla S & Spindler-Barth M (2002) Ligand-induced heterodimerization between the ligand binding domains of the *Drosophila* ecdysteroid receptor and ultraspiracle. *Eur J Biochem* **269**, 3237–3245.

26 Dues G, Müller S & Johnsson N (2001) Detection of a conformational change in Gγ upon binding Gβ in living cells. *FEBS Lett* **505**, 75–80.

27 Raquet X, Eckert JH, Müller S & Johnsson N (2001) Detection of altered protein conformations in living cells. *J Mol Biol* **305**, 927–938.

28 Johnsson N (2002) A split-ubiquitin-based assay detects the influence of mutations on the conformational stability of the p53 DNA binding domain *in vivo*. *FEBS Lett* **531**, 259–264.

29 Vögler O, Barceló JM, Ribas C & Escribá PV (2008) Membrane interactions of G proteins and other related proteins. *Biochim Biophys Acta* **1778**, 1640–1652.

30 Dechant R & Peter M (2008) Nutrient signals driving cell growth. *Curr Opin Cell Biol* **20**, 678–687.

31 Zaman S, Lippman SI, Zhao X & Broach JR (2008) How *Saccharomyces* responds to nutrients. *Annu Rev Genet* **42**, 27–81.

32 Elion EA (2000) Pheromone response, mating and cell biology. *Curr Opin Microbiol* **3**, 573–581.

33 Tomizaki K, Usui K & Mihara H (2010) Protein–protein interactions and selection: array-based

techniques for screening disease-associated biomarkers in predictive/early diagnosis. *FEBS J* **277**, 1996–2005.
34 Umetsu M, Nakanishi T, Asano R, Hattori T & Kumagai I (2010) Protein–protein interactions and selection: generation of molecule-binding proteins on the basis of tertiary structural information. *FEBS J* **277**, 2006–2014.
35 Tisi R, Belotti F, Paiardi C, Brunetti F & Martegani E (2008) The budding yeast RasGEF Cdc25 reveals an unexpected nuclear localization. *Biochim Biophys Acta* **1783**, 2363–2374.
36 Aronheim A, Zandi E, Hennemann H, Elledge SJ & Karin M (1997) Isolation of an AP-1 repressor by a novel method for detecting protein–protein interactions. *Mol Cell Biol* **17**, 3094–3102.
37 Aronheim A (1997) Improved efficiency Sos recruitment system: expression of the mammalian GAP reduces isolation of Ras GTPase false positives. *Nucleic Acids Res* **25**, 3373–3374.
38 Broder YC, Katz S & Aronheim A (1998) The Ras recruitment system, a novel approach to the study of protein–protein interactions. *Curr Biol* **8**, 1121–1124.
39 Gunde T & Barberis A (2005) Yeast growth selection system for detecting activity and inhibition of dimerization-dependent receptor tyrosine kinase. *BioTechniques* **39**, 541–549.
40 Ecker K, Lorenz A, Wolf F, Ploner C, Böck G, Duncan T, Geley S & Helmberg A (2009) A RAS recruitment screen identifies ZKSCAN4 as a glucocorticoid receptor-interacting protein. *J Mol Endocrinol* **42**, 105–117.
41 Manahan CL, Patnana M, Blumer KJ & Linder ME (2000) Dual lipid modification motifs in Gα and Gγ subunits are required for full activity of the pheromone response pathway in *Saccharomyces cerevisiae*. *Mol Biol Cell* **11**, 957–968.
42 Hirschman JE & Jenness DD (1999) Dual lipid modification of the yeast Gγ subunit Ste18p determines membrane localization of Gβγ. *Mol Cell Biol* **19**, 7705–7711.
43 Dosil M, Schandel KA, Gupta E, Jenness DD & Konopka JB (2000) The C terminus of the *Saccharomyces cerevisiae* α-factor receptor contributes to the formation of preactivation complexes with its cognate G protein. *Mol Cell Biol* **20**, 5321–5329.
44 Leberer E, Thomas DY & Whiteway M (1997) Pheromone signalling and polarized morphogenesis in yeast. *Curr Opin Genet Dev* **7**, 59–66.
45 Leeuw T, Wu CL, Schrag JD, Whiteway M, Thomas DY & Leberer E (1998) Interaction of a G-protein β-subunit with a conserved sequence in Ste20/PAK family protein kinases. *Nature* **391**, 191–195.
46 Elion EA (2001) The Ste5p scaffold. *J Cell Sci* **114**, 3967–3978.
47 Pryciak PM & Huntress FA (1998) Membrane recruitment of the kinase cascade scaffold protein Ste5 by the Gβγ complex underlies activation of the yeast pheromone response pathway. *Genes Dev* **12**, 2684–2697.
48 Chang F & Herskowitz I (1990) Identification of a gene necessary for cell cycle arrest by a negative growth factor of yeast: FAR1 is an inhibitor of a G1 cyclin, CLN2. *Cell* **63**, 999–1011.
49 Chang F & Herskowitz I (1992) Phosphorylation of FAR1 in response to alpha-factor: a possible requirement for cell-cycle arrest. *Mol Biol Cell* **3**, 445–450.
50 McKinney JD & Cross FR (1995) *FAR1* and the G1 phase specificity of cell cycle arrest by mating factor in *Saccharomyces cerevisiae*. *Mol Cell Biol* **15**, 2509–2516.
51 Dolan JW, Kirkman C & Fields S (1989) The yeast STE12 protein binds to the DNA sequence mediating pheromone induction. *Proc Natl Acad Sci USA* **86**, 5703–5707.
52 Song D, Dolan JW, Yuan YL & Fields S (1991) Pheromone-dependent phosphorylation of the yeast STE12 protein correlates with transcriptional activation. *Genes Dev* **5**, 741–750.
53 McCaffrey G, Clay FJ, Kelsay K & Sprague GF Jr (1987) Identification and regulation of a gene required for cell fusion during mating of the yeast *Saccharomyces cerevisiae*. *Mol Cell Biol* **7**, 2680–2690.
54 Hagen DC, McCaffrey G & Sprague GF Jr (1991) Pheromone response elements are necessary and sufficient for basal and pheromone-induced transcription of the *FUS1* gene of *Saccharomyces cerevisiae*. *Mol Cell Biol* **11**, 2952–2961.
55 Dohlman HG, Song J, Ma D, Courchesne WE & Thorner J (1996) Sst2, a negative regulator of pheromone signalling in the yeast *Saccharomyces cerevisiae*: expression, localization, and genetic interaction and physical association with Gpa1 (the G-protein α subunit). *Mol Cell Biol* **16**, 5194–5209.
56 Apanovitch DM, Slep KC, Sigler PB & Dohlman HG (1998) Sst2 is a GTPase-activating protein for Gpa1: purification and characterization of a cognate RGS–Gα protein pair in yeast. *Biochemistry* **37**, 4815–4822.
57 Heilker R, Wolff M, Tautermann CS & Bieler M (2009) G-protein-coupled receptor-focused drug discovery using a target class platform approach. *Drug Discov Today* **14**, 231–240.
58 Williams C & Hill SJ (2009) GPCR signalling: understanding the pathway to successful drug discovery. *Methods Mol Biol* **552**, 39–50.
59 Minic J, Sautel M, Salesse R & Pajot-Augy E (2005) Yeast system as a screening tool for pharmacological assessment of g protein coupled receptors. *Curr Med Chem* **12**, 961–969.

60 Ladds G, Goddard A & Davey J (2005) Functional analysis of heterologous GPCR signalling pathways in yeast. *Trends Biotechnol* **23**, 367–373.

61 Martin NP, Celić A & Dumont ME (2002) Mutagenic mapping of helical structures in the transmembrane segments of the yeast alpha-factor receptor. *J Mol Biol* **317**, 765–788.

62 Clark CD, Palzkill T & Botstein D (1994) Systematic mutagenesis of the yeast mating pheromone receptor third intracellular loop. *J Biol Chem* **269**, 8831–8841.

63 Dube P, DeCostanzo A & Konopka JB (2000) Interaction between transmembrane domains five and six of the α-factor receptor. *J Biol Chem* **275**, 26492–26499.

64 Hauser M, Kauffman S, Lee BK, Naider F & Becker JM (2007) The first extracellular loop of the *Saccharomyces cerevisiae* G protein-coupled receptor Ste2p undergoes a conformational change upon ligand binding. *J Biol Chem* **282**, 10387–10397.

65 Ongay-Larios L, Saviñón-Tejeda AL, Williamson MJ Jr, Durán-Avelar M & Coria R (2000) The Leu-132 of the Ste4(Gβ) subunit is essential for proper coupling of the G protein with the Ste2 α factor receptor during the mating pheromone response in yeast. *FEBS Lett* **467**, 22–26.

66 Manfredi JP, Klein C, Herrero JJ, Byrd DR, Trueheart J, Wiesler WT, Fowlkes DM & Broach JR (1996) Yeast α mating factor structure–activity relationship derived from genetically selected peptide agonists and antagonists of Ste2p. *Mol Cell Biol* **16**, 4700–4709.

67 Ishii J, Matsumura S, Kimura S, Tatematsu K, Kuroda S, Fukuda H & Kondo A (2006) Quantitative and dynamic analyses of G protein-coupled receptor signalling in yeast using Fus1, enhanced green fluorescence protein (EGFP), and His3 fusion protein. *Biotechnol Prog* **22**, 954–960.

68 Minic J, Persuy MA, Godel E, Aioun J, Connerton I, Salesse R & Pajot-Augy E (2005) Functional expression of olfactory receptors in yeast and development of a bioassay for odorant screening. *FEBS J* **272**, 524–537.

69 Ishii J, Tanaka T, Matsumura S, Tatematsu K, Kuroda S, Ogino C, Fukuda H & Kondo A (2008) Yeast-based fluorescence reporter assay of G protein-coupled receptor signalling for flow cytometric screening: *FAR1*-disruption recovers loss of episomal plasmid caused by signalling in yeast. *J Biochem* **143**, 667–674.

70 King K, Dohlman HG, Thorner J, Caron MG & Lefkowitz RJ (1990) Control of yeast mating signal transduction by a mammalian β_2-adrenergic receptor and G_s α subunit. *Science* **250**, 121–123.

71 Erlenbach I, Kostenis E, Schmidt C, Hamdan FF, Pausch MH & Wess J (2001) Functional expression of M_1, M_3 and M_5 muscarinic acetylcholine receptors in yeast. *J Neurochem* **77**, 1327–1337.

72 Li B, Scarselli M, Knudsen CD, Kim SK, Jacobson KA, McMillin SM & Wess J (2007) Rapid identification of functionally critical amino acids in a G protein-coupled receptor. *Nat Methods* **4**, 169–174.

73 Brown AJ, Dyos SL, Whiteway MS, White JH, Watson MA, Marzioch M, Clare JJ, Cousens DJ, Paddon C, Plumpton C *et al.* (2000) Functional coupling of mammalian receptors to the yeast mating pathway using novel yeast/mammalian G protein α-subunit chimeras. *Yeast* **16**, 11–22.

74 Leplatois P, Josse A, Guillemot M, Febvre M, Vita N, Ferrara P & Loison G (2001) Neurotensin induces mating in *Saccharomyces cerevisiae* cells that express human neurotensin receptor type 1 in place of the endogenous pheromone receptor. *Eur J Biochem* **268**, 4860–4867.

75 Price LA, Kajkowski EM, Hadcock JR, Ozenberger BA & Pausch MH (1995) Functional coupling of a mammalian somatostatin receptor to the yeast pheromone response pathway. *Mol Cell Biol* **15**, 6188–6195.

76 Pausch MH, Lai M, Tseng E, Paulsen J, Bates B & Kwak S (2004) Functional expression of human and mouse P2Y12 receptors in *Saccharomyces cerevisiae*. *Biochem Biophys Res Commun* **324**, 171–177.

77 Klein C, Paul JI, Sauvé K, Schmidt MM, Arcangeli L, Ransom J, Trueheart J, Manfredi JP, Broach JR & Murphy AJ (1998) Identification of surrogate agonists for the human FPRL-1 receptor by autocrine selection in yeast. *Nat Biotechnol* **16**, 1334–1337.

78 Medici R, Bianchi E, Di Segni G & Tocchini-Valentini GP (1997) Efficient signal transduction by a chimeric yeast–mammalian G protein α subunit Gpa1–Gsα covalently fused to the yeast receptor Ste2. *EMBO J* **16**, 7241–7249.

79 Ehrhard KN, Jacoby JJ, Fu XY, Jahn R & Dohlman HG (2000) Use of G-protein fusions to monitor integral membrane protein–protein interactions in yeast. *Nat Biotechnol* **18**, 1075–1079.

80 Fukuda N, Ishii J, Tanaka T, Fukuda H & Kondo A (2009) Construction of a novel detection system for protein–protein interactions using yeast G-protein signalling. *FEBS J* **276**, 2636–2644.

81 Nilsson B, Moks T, Jansson B, Abrahmsén L, Elmblad A, Holmgren E, Henrichson C, Jones TA & Uhlén M (1987) A synthetic IgG-binding domain based on staphylococcal protein A. *Protein Eng* **1**, 107–113.

82 Cedergren L, Andersson R, Jansson B, Uhlén M & Nilsson B (1993) Mutational analysis of the interaction between staphylococcal protein A and human IgG1. *Protein Eng* **6**, 441–448.

83 Jendeberg L, Persson B, Andersson R, Karlsson R, Uhlén M & Nilsson B (1995) Kinetic analysis of the interaction between protein A domain variants and

human Fc using plasmon resonance detection. *J Mol Recognit* **8**, 270–278.

84 Yu X, Wu LC, Bowcock AM, Aronheim A & Baer R (1998) The C-terminal (BRCT) domains of BRCA1 interact *in vivo* with CtIP, a protein implicated in the CtBP pathway of transcriptional repression. *J Biol Chem* **273**, 25388–25392.

85 Huang W, Zhou X, Lefebvre V & de Crombrugghe B (2000) Phosphorylation of SOX9 by cyclic AMP-dependent protein kinase A enhances SOX9's ability to transactivate a *Col2a1* chondrocyte-specific enhancer. *Mol Cell Biol* **20**, 4149–4158.

86 Schwarzer C, Barnikol-Watanabe S, Thinnes FP & Hilschmann N (2002) Voltage-dependent anion-selective channel (VDAC) interacts with the dynein light chain Tctex1 and the heat-shock protein PBP74. *Int J Biochem Cell Biol* **34**, 1059–1070.

87 Chomchan P, Li SF & Shirako Y (2003) Rice grassy stunt tenuivirus nonstructural protein p5 interacts with itself to form oligomeric complexes in vitro and in vivo. *J Virol* **77**, 769–775.

88 Keller CA, Yuan X, Panzanelli P, Martin ML, Alldred M, Sassoè-Pognetto M & Lüscher B (2004) The γ2 subunit of $GABA_A$ receptors is a substrate for palmitoylation by GODZ. *J Neurosci* **24**, 5881–5891.

89 Kaiser C & James SR (2004) Acetylation of insulin receptor substrate-1 is permissive for tyrosine phosphorylation. *BMC Biol* **2**, 23, doi:10.1186/1741-7007-2-23.

90 Hanamoto T, Ozaki T, Furuya K, Hosoda M, Hayashi S, Nakanishi M, Yamamoto H, Kikuchi H, Todo S & Nakagawara A (2005) Identification of protein kinase A catalytic subunit beta as a novel binding partner of p73 and regulation of p73 function. *J Biol Chem* **280**, 16665–16675.

91 Detka D, Kalita K & Kaczmarek L (2006) Activation function 1 domain plays a negative role in dimerization of estrogen receptor beta. *J Steroid Biochem Mol Biol* **99**, 157–160.

92 Georgiakaki M, Chabbert-Buffet N, Dasen B, Meduri G, Wenk S, Rajhi L, Amazit L, Chauchereau A, Burger CW, Blok LJ *et al.* (2006) Ligand-controlled interaction of histone acetyltransferase binding to ORC-1 (HBO1) with the N-terminal transactivating domain of progesterone receptor induces steroid receptor coactivator 1-dependent coactivation of transcription. *Mol Endocrinol* **20**, 2122–2140.

93 Kim MJ, Kim HR & Paek KH (2006) Arabidopsis tonoplast proteins TIP1 and TIP2 interact with the cucumber mosaic virus 1a replication protein. *J Gen Virol* **87**, 3425–3431.

94 Carpentier I, Coornaert B & Beyaert R (2008) Smurf2 is a TRAF2 binding protein that triggers TNF-R2 ubiquitination and TNF-R2-induced JNK activation. *Biochem Biophys Res Commun* **374**, 752–757.

95 Liu M & Gelli A (2008) Elongation factor 3, EF3, associates with the calcium channel Cch1 and targets Cch1 to the plasma membrane in *Cryptococcus neoformans*. *Eukaryot Cell* **7**, 1118–1126.

96 Aronheim A, Broder YC, Cohen A, Fritsch A, Belisle B & Abo A (1998) Chp, a homologue of the GTPase Cdc42Hs, activates the JNK pathway and is implicated in reorganizing the actin cytoskeleton. *Curr Biol* **8**, 1125–1128.

97 Takemaru KI & Moon RT (2000) The transcriptional coactivator CBP interacts with beta-catenin to activate gene expression. *J Cell Biol* **149**, 249–254.

98 Holmberg C, Katz S, Lerdrup M, Herdegen T, Jäättelä M, Aronheim A & Kallunki T (2002) A novel specific role for IκB kinase complex-associated protein in cytosolic stress signaling. *J Biol Chem* **277**, 31918–31928.

99 Köhler F & Müller KM (2003) Adaptation of the Ras-recruitment system to the analysis of interactions between membrane-associated proteins. *Nucleic Acids Res* **31**, e28, doi:10.1093/nar/gng028.

100 Hennemann H, Vassen L, Geisen C, Eilers M & Möröy T (2003) Identification of a novel Krüppel-associated box domain protein, Krim-1, that interacts with c-Myc and inhibits its oncogenic activity. *J Biol Chem* **278**, 28799–28811.

101 Frankel P, Aronheim A, Kavanagh E, Balda MS, Matter K, Bunney TD & Marshall CJ (2005) RalA interacts with ZONAB in a cell density-dependent manner and regulates its transcriptional activity. *EMBO J* **24**, 54–62.

102 Fukuda N, Ishii J, Tanaka T & Kondo A (2010) The competitor-introduced Gγ recruitment system, a new approach to screen affinity-enhanced proteins. *FEBS J* **277**, 1704–1712.

Biochemical Engineering Journal 48 (2010) 416–423

Contents lists available at ScienceDirect

Biochemical Engineering Journal

journal homepage: www.elsevier.com/locate/bej

Review

Potential uses of titanium dioxide in conjunction with ultrasound for improved disinfection

Nobuaki Shimizu[a,b,*], Kazuaki Ninomiya[a,b], Chiaki Ogino[c], Mohammad Mizanur Rahman[b]

[a] Division of Biological Measurement and Applications, Institute of Nature and Environmental Technology, Kanazawa University, Kanazawa 920-1192, Japan
[b] Division of Material Engineering, Graduate School of Natural Science and Technology, Kanazawa University, Kanazawa 920-1192, Japan
[c] Department of Chemical Science and Engineering, Graduate School of Engineering, Kobe University, Kobe 657-8501, Japan

ARTICLE INFO

Article history:
Received 28 July 2009
Received in revised form 8 October 2009
Accepted 11 October 2009

Keywords:
Disinfection
Titanium dioxide
Ultrasonic irradiation
Hydroxyl radical
Cavitation

ABSTRACT

The inactivation of hazardous microorganisms is an important subject for water treatment. While the most widely used methods in water treatment systems are chlorination, ozonation, and ultraviolet ray irradiation, the drawbacks of these techniques surpass their efficacy. The potential formation of carcinogenic chemical byproducts has been reported as a drawback of chemical disinfection methods, hence there is a need to develop some alternate disinfection techniques. Ultrasonic (US) irradiation is well known as a useful technique for microbial inactivation due to its chemical and physical factors. Our recent studies indicated that the presence of titanium dioxide (TiO_2), known as a photocatalyst, accelerates the generation of hydroxyl (OH) radicals during US irradiation, and that the process is mediated through the induction of cavitation bubbles in irradiating solutions. This review describes a disinfection method that utilizes US irradiation of contaminated solution in the presence of TiO_2, a so-called "sonocatalytic disinfection" method. The significant role of OH radicals in the mechanism of cell-killing is discussed.

Contents

* Corresponding author at: Division of Biological Measurement and Applications, Institute of Nature and Environmental Technology, Kanazawa University, Kanazawa 920-1192, Japan. Tel.: +81 76 234 4807; fax: +81 76 234 4829.
E-mail address: nshimizu@t.kanazawa-u.ac.jp (N. Shimizu).

1369-703X/$ – see front matter © 2009 Elsevier B.V. All rights reserved.
doi:10.1016/j.bej.2009.10.009

1. Introduction

While water has been disinfected by various chemical and physical methods, the drawbacks of these techniques surpass their efficacy [1–4]. Chlorine has been used widely as a disinfectant, but it results in the formation of mutagenic and carcinogenic compounds in water and wastewater effluent [5,6]. Further, some microorganisms produce colonies and spores that agglomerate in large clusters. Chemical treatment of such clusters may kill microorganisms on the surface but leave the organisms under the surface intact. In the case of ultraviolet (UV) light, disinfection is affected by suspended solid particles, because microorganisms can be shielded from UV light and the formation of organic fouling on the UV lamps suppresses disinfection [7,8]. Thus, there is a need to develop some alternate techniques for water disinfection.

An ultrasonic (US) system has been used as an alternative disinfection method and has been used to oxidize contaminants in water as well as to inactivate cells [9–16]. US has been found capable of producing cell lysis and other damaging effects, such as membrane impairment, DNA degradation, organelle damage, and miscellaneous functional and biochemical changes. As illustrated in Fig. 1(A), mechanism for the inactivation of microbial cells by the US system is based on the acoustic cavitations created as a result of the growth and adiabatic collapse of bubbles in the liquid. As a result of cavitational bubble implosions, extreme temperatures and pressures are generated at the center of the collapsed bubble. One of the factors for microbial inactivation is these extreme temperatures and pressures ("physical factor" in Fig. 1(A)). Another factor for microbial inactivation is hydroxyl (OH) radicals, hydrogen peroxide, and other oxidants produced via dissociation of water molecules caused by extreme temperatures in the collapsed bubble ("chemical factor" in Fig. 1(A)) [17–19].

Recently, Shimizu and co-workers [20–22] reported that microbial cells were inactivated more effectively by US irradiation with addition of titanium dioxide (TiO_2), and that the OH radical has been shown to be responsible for the sterilization effect. This review therefore focused the disinfection by this US/TiO_2 system, and summarized the following points; the enhancement of the OH radical generation by the US/TiO_2 system, the applicability of this US/TiO_2 system to degradation of organic compound and inactivation of microbial cells, membrane damage of microbial cells by US/TiO_2 system, and the possible mechanism of OH radical generation and microbial inactivation by the US/TiO_2 system.

2. Generation of OH radicals during US irradiation in the presence of TiO_2

The TiO_2 photocatalyst has been used in the degradation of different chemicals under UV light illumination since the first report of Fujishima et al. on the application of semiconductors to oxidation processes [27]. Those findings indicated that TiO_2 can catalyze the production of OH radicals and other oxidizing agents on its surface in photochemical reactions [28–31].

The application of TiO_2 under US seemed to be an efficient method for enhancing the degradation of hazardous materials [24–26]. While the detailed mechanisms have not been clarified yet, the possible roles of OH radicals in the US/TiO_2-induced degradation of hazardous materials were proposed using several OH radical scavenging agents. These agents significantly suppressed degradation, possibly due to the quenching of the OH radicals. While these results may indicate the possibility that OH radicals play important roles in degradation mechanisms, the successful application of TiO_2 in the US system first requires the clarification of the augmentation of OH radical formation in this system.

2.1. Effect of TiO_2 addition on OH radical generation under US irradiation

The OH radical has a very short half-life due to its high reactivity, and is present at extremely low concentrations. Therefore, in general, OH radical generation has been evaluated based on the measurement of aromatic molecules hydroxylated by OH radical using HPLC-ECD [32,33]. Salicylic acid has been mainly used as highly selective OH radical trapping reagent, because of the high reaction rate ($2.7 \times 10^{10}\ M^{-1}\ s^{-1}$) [34] and the stability of result-

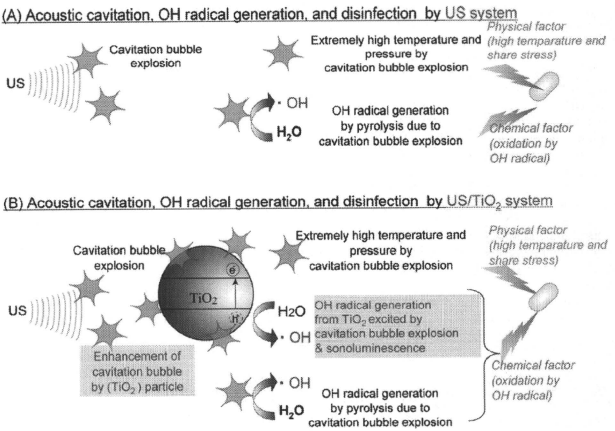

Fig. 1. Conceptual illustration for the mechanism of cavitation bubble formation and implosion, OH radical generation, and microbial inactivation by US system (A) and US/TiO_2 system (B).

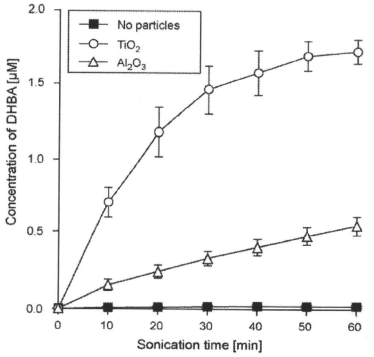

Fig. 2. Changes in DHBA concentrations during 60 min of US irradiation in the presence of TiO_2, Al_2O_3, or neither [35].

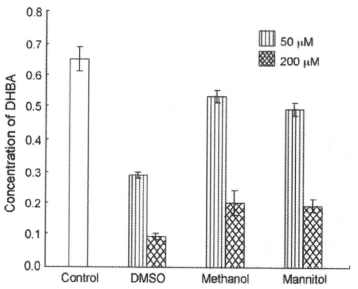

Fig. 3. Significant suppression of DHBA formation by several OH radical scavenging compounds [35]. The concentration of DHBA was measured after 10 min US irradiation with TiO_2 and salicylic acid in the presence of DMSO, methanol, or mannitol. The control indicates US irradiation with TiO_2 and salicylic acid in the absence of scavenger.

ing hydroxylated products 2,3-dihydroxybenzoic acid (DHBA) and 2,5-DHBA.

To evaluate effect of TiO_2 addition on the OH radical generation under US irradiation, the time course of the total DHBA concentration (2,3-DHBA plus 2,5-DHBA) was studied by irradiating US (frequency of 36 kHz and with a rated output power of 200 W) to the salicylic acid solution with addition of TiO_2 (2.0 mm diameter). Moreover, total DHBA concentration in the presence of TiO_2 was compared with that in the presence of Al_2O_3 (2.0 mm diameter) in order to elucidate the specificity of the sonocatalytic effects of TiO_2 [35]. As shown in Fig. 2, total concentration of DHBA changed only slightly in the absence of any particles (0.02 μM after 60 min irradiation). However in the presence of TiO_2, total DHBA concentration increased significantly with elapsed time of US irradiation, reaching plateau of 1.73 μM after 60 min. DHBA formation was significant also in the presence of Al_2O_3 particles, and the total concentration of DHBA was 0.54 μM at the 60-min irradiation period. However, the increased level was significantly lower than that of the concentration induced by TiO_2. These results demonstrate that the combination of TiO_2 plus US plays a specific role in the generation of OH radicals.

2.2. Effects of OH radical scavengers on OH radical generation by US/TiO_2 system

The oxidation mechanism was studied by employing the selected radical scavengers for this process. Dimethylsulfoxide (DMSO), methanol, and mannitol were tested as OH radical scavengers to evaluate the role of OH radicals in the oxidation of salicylic acid [36–38]. Fig. 3 compares the total concentration of DHBA produced after a 10-min irradiation period in the presence of each of these scavengers. The addition of each scavenger into the irradiating solution suppressed the formation of DHBA significantly. DMSO had the highest suppressive effect, at 200 μM. These results suggested that OH radicals were surely generated by the US/TiO_2 system.

2.3. Effects of deaeration on OH radical generation by US/TiO_2 system

The next experiment was conducted to determine whether or not the deaeration of the salicylate solution affected DHBA formation. Fig. 4 indicates the effect of deaeration pressure on the dissolved oxygen (DO) concentration (A) and the formation of DHBA (B) measured at 30 min after sonication began. The DO concentration of air-saturated aqueous solution was 8.5 ppm, which decreased linearly as the deaeration pressure increased. The DO concentration became almost null after 96 kPa negative pressure was applied for 30 min. The DHBA concentration decreased linearly as the deaeration pressure increased, and became almost null after 96 kPa negative pressure was applied. From the data in Fig. 4, the deaeration pressures corresponding to the half-decay concentration of DO and DHBAs were estimated to be 50.0 and 51.3 kPa, respectively. These results suggest that the formation of cavitation bubbles may play an important role in the formation of OH radicals by the US/TiO_2 system.

2.4. Effects of dissolved gases on OH radical generation by US/TiO_2 system

The phenomenon of acoustic cavitation – the nucleation, growth, and collapse of small gas bubbles in liquids – is the basis of a variety of US-induced mechanical and chemical processes [18]. It is recognized that the core temperatures of cavitation bubbles are very high (several thousand Kelvin) and are affected by the properties of the gases dissolved in aqueous solution. Assuming an adiabatic collapse, the final temperature of the gas bubble (T_{ad}) can be estimated by the following equation [19]:

$$T_{ad} = T\left(\frac{R_{init}}{R_{fin}}\right)^{3(\gamma-1)}$$

where T is the temperature of the liquid, ($\gamma = C_p/C_v$) is the ratio of the specific heat at constant pressure to the specific heat at constant volume of the gas inside the bubble, and R_{init} is the initial radius of a bubble that collapses to a final radius of R_{fin}. To clarify the hypothesis that the core temperature of the cavitation bubbles may affect the sonocatalytic formation of OH radicals, we examined Xe, Ar, O_2, and N_2 with different γ values. It can be seen that the power of the dissolved gases on the formation of OH radicals was in the order Xe > Ar > O_2 > N_2. This order was consistent with the previous results of sonoluminescence [19]. Our results suggest the possibility that cavitation bubbles that collapse at higher temperature are more effective for the sonocatalytic formation of OH radicals with TiO_2. The γ values for Xe, Ar, O_2, and N_2 are 1.66, 1.67, 1.40, and 1.40, respectively. Because there

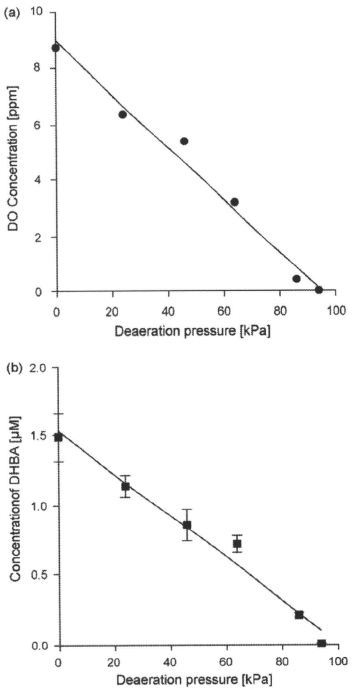

Fig. 4. The effects of deaeration pressure on the concentrations of dissolved oxygen (DO) and DHBA [35]. DO concentration (A) or formation of DHBAs (B) was measured at 30 min after the initiation of sonication.

are few differences between γ values for Xe and Ar, the final temperature seems to be almost the same under Xe and Ar atmospheres, although OH radical formation was significantly higher in the former than in the latter. Cavitation thresholds increase with increasing frequency, ambient pressure, and liquid viscosity but decrease with increasing gas content and liquid temperature [39]. The solubility of Xe is three times that of Ar, which also supports the present results, thus suggesting that OH radical formation was significantly higher under the Xe atmosphere than under the Ar atmosphere. These results also suggest that cavitation bubbles implosion may be a key for OH radical generation by the US/TiO_2 system.

3. Applicability of US/TiO_2 system to the degradation of organic compounds and microorganisms

The combined irradiation of UV and US toward TiO_2 seems to enhance the degradation ratio of organic pollutants due to the increase in the generation of OH radicals. In fact, the combination of UV and US irradiation has been reported to have a positive effect on the degradation ratio of the hazardous chemical substances in the presence of TiO_2 [40–43]. For example, it was demonstrated that the US had a synergistic effect on the photocatalytic degradation of salicylic acid and formic acid [42], while the detailed mechanisms have not been clarified yet.

Recent observations have indicated that TiO_2 particles can enhance the oxidizing power of US even in the absence of UV irradiation [25,26]. In the following sections, applied studies of this US/TiO_2 system to the degradation of chemical substance and microbial inactivation were presented, and it was discussed that the OH radical generated by US/TiO_2 system was contributed to the disinfection.

3.1. Degradation of methylene blue by US/TiO_2 system

Following US irradiation to methylene blue solution containing TiO_2 (2 g/ml) and H_2O_2 (50 mM), the temporal changes in the spectral features of the solution were studied by monitoring the absorbance of UV–vis spectra at 665 nm [45]. Fig. 5 shows a typical absorption spectral pattern and photographs of the methylene blue solution (0.3 mM). US irradiation for 30 min significantly decreased absorbance at 665 nm, and absorbance almost disappeared after 60-min irradiation (Fig. 5(A)). As shown in Fig. 5(B), the color of the methylene blue solution containing TiO_2 and subjected to 60-min irradiation faded completely, whereas the solution of methylene blue containing Al_2O_3 showed no significant color change. This result suggested that the combination of TiO_2 plus US plays a specific role in the degradation of methylene blue. This effect could not be attributed to the adsorption of methylene blue on the surface of TiO_2 because there was no significant reduction in the methylene blue concentration during several days of incubation in the presence of TiO_2 and without any treatment. These results further indicated that the addition of H_2O_2 to the solution enhanced methylene blue degradation, and this may have been due to the fact that H_2O_2 was a more effective electron acceptor than O_2 in the solution.

3.2. Inactivation of *Legionella* by US/TiO_2 system

Diluted cell suspension of *Legionella* was treated in an US bath in the presence or absence of TiO_2 [21]. The concentrations of viable cells were then measured, based on the number of colonies formed on BCYE plates. Fig. 6 shows the effect of the presence of TiO_2 on the concentration of viable cells after the US treatment. Inactivation of *Legionella* in the absence of TiO_2 indicated that only 18% of the initial viable cells were killed after 30 min of treatment. However, the addition of TiO_2 pellets to the solutions significantly increased the disinfection power. The concentration of viable cells was reduced to 3% of the initial value in the presence of 1.0 g/ml TiO_2 after a 30-min treatment period. This enhancing effect cannot be attributed to the aggregation or adsorption of cells. When no treatment was provided, there was no reduction in cell concentrations during the incubation of *Legionella* in the presence of TiO_2.

Disinfection efficiency in the presence of TiO_2 was compared with that in the presence of Al_2O_3 in order to elucidate the specificity of the sonocatalytic effects of TiO_2. The same size and amount of Al_2O_3 pellets (diameter = 2.0 mm) that were used for TiO_2 were added to the treatment solutions, followed by a 15-min treatment period. Fig. 7 shows the relative concentrations of viable cells after 15 min of treatment in the presence of 0.3 g/ml of Al_2O_3 and TiO_2. These results indicate that the inactivation efficiency of *Legionella* was larger in the presence of TiO_2 compared with that in the presence of Al_2O_3, indicating that there is the sonocatalytic effects observed specifically in the case of TiO_2. The possible scenario for the sonocatalytic effect will be explained in the following section.

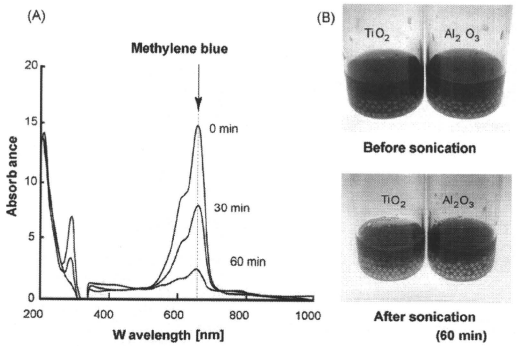

Fig. 5. (A) Temporal spectral changes in methylene blue solution containing TiO_2 and H_2O_2 under US irradiation [45]. The 665 nm absorption band was selected to monitor the temporal concentration changes of methylene blue dye. (B) Degradation of methylene blue solution containing TiO_2 pellets after 60-min US irradiation.

3.3. *Effects of radical scavenging compounds*

The mechanism of microbial inactivation by US/TiO_2 system was investigated by examining the effects of selected radical scavengers on the cell-killing process. It has been reported that glutathione can inhibit the photodynamic DNA strand-breaking activity of TiO_2 [46]. In addition, an *in vivo* elevation in glutathione concentrations in the rat brain has been reported to reduce the protein oxidation induced by OH radicals [47]. Therefore, glutathione was tested as a scavenger of OH radicals to evaluate the role of such radicals in this process. Different concentrations of this glutathione were added to the treatment solutions, and *Legionella* concentrations were measured after a 15-min treatment period. The results clearly show that the presence of glutathione suppresses the disinfection process at concentrations above 10 mM and that the scavenging effect is proportional to the concentration of glutathione in the applied range (data not shown). From these results, it was confirmed that the OH radical generation by US/TiO_2 system was contributed to the microbial inactivation, as suggested in Fig. 1(B).

4. Microbial membrane damage following disinfection by US/TiO_2 system

Maness and co-workers [23] reported for the first time that the lipid peroxidation reaction is the mechanism underlying the death of *E. coli* by photocatalytic TiO_2 reaction. Therefore, microbial membrane damage and DNA leakage during disinfection by sonocatalytic TiO_2 reaction was examined to investigate the killing mechanisms.

4.1. *Membrane damage by US/TiO_2 system*

To investigate damage of cellular membrane by US/TiO_2 system, a fluorogenic assay method was applied and the release of 4-methyl-7-hydroxycoumarin upon cell lysis was measured by a fluorescence spectrophotometer [22]. In this method, 4-methylumbelliferyl-β-D-glucuronide (MUG) was added to *E. coli* culture and was incubated at 37 °C for 4 h. MUG was taken up by *E. coli*

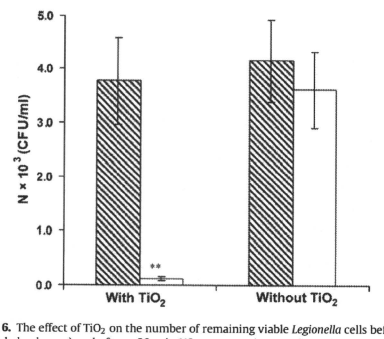

Fig. 6. The effect of TiO_2 on the number of remaining viable *Legionella* cells before (shaded columns) and after a 30-min US treatment (open columns) at a concentration of TiO_2 of 1.0 g/ml [21]. **Significantly different from the control ($p < 0.01$, one-way ANOVA).

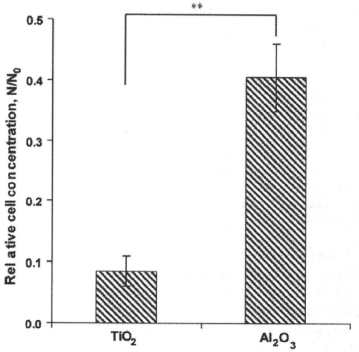

Fig. 7. Inactivation of *Legionella* in the presence of Al_2O_3 or TiO_2 after a 15-min treatment period [21]. Initial cell concentration, 4.0×10^3 CFU/ml. **$p < 0.01$ (one-way ANOVA).

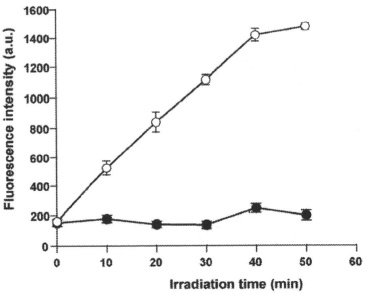

Fig. 8. The effects of TiO_2 on the release of 4-methyl-7-hydroxycoumarin during US irradiation of *E. coli* solution [22]. Open circles, US irradiation in the presence of TiO_2; filled circles, US irradiation without TiO_2.

during this period and converted to 4-methyl-7-hydroxycoumarin by β-glucuronidase intracellularly. This compound has fluorescent characteristics and can be detected by a fluorescence spectrophotometer upon leakage from *E. coli* cells. Fig. 8 shows the variation in the fluorescence intensity of irradiated samples during US irradiation that indicates the leakage of this compound into the solutions. US irradiation in the absence of TiO_2 was found to have no considerable increase in the amount of leaked fluorescent agent. Also, the results obtained in the blank samples containing TiO_2 and in the silent condition did not show any cell lysis during the incubation period. However, the amount of 4-methyl-7-hydroxycoumarin leaked during the irradiation period in the presence of TiO_2 was increased significantly, suggesting a high cell lysis rate under this condition.

4.2. Leakage and subsequent degradation of DNA by US/TiO_2 system

The effect of TiO_2 on cell lysis was further studied by analyzing the leakage and the subsequent degradation of DNA during US irradiation. Sonicated samples were pretreated to separate the leaked DNA and then were analyzed by agarose gel electrophoresis. The results of electrophoresis are shown in Fig. 9, which compares DNA fragments obtained in the samples, which were irradiated ultrasonically in the presence of TiO_2, with the extracted intact DNA of *E. coli*. DNA leakage and degradation were obvious during the irradiation period, and the resultant fragments indicated that the degradation was preceded by an irradiation period. This may be an indicative of a high rate of cell lysis during US irradiation in the presence of TiO_2. DNA fragmentation was clearly taking place within 5 min of irradiation, after which the degradation of DNA resulted in smaller fragments. This amount of degradation indicates a high ratio of cell lysis during the 5-min irradiation period, compatible with the high ratio of cell-killing under these conditions.

The results of electrophoresis were compared with the samples that were irradiated ultrasonically with no particles. US irradiation's effect on the release and degradation of DNA was not significant in the samples containing no particles. In addition, the results indicate that US irradiation to *E. coli* in the presence of Al_2O_3 resulted in cell lysis followed by degradation of leaked DNA during the irradiation period. Al_2O_3 particles may also induce a high degree of cavitation in the US system, resulting in high rates of cell lysis and disinfection. However, TiO_2 particles have been reported

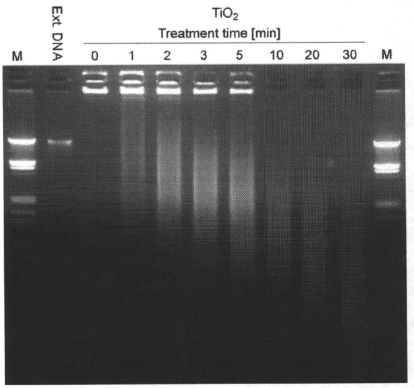

Fig. 9. Agarose gel electrophoresis analysis of DNA leaked from *E. coli* during US irradiation in the presence of TiO_2 [22]. Initial concentration of *E. coli* was 3.8×10^8 cells/ml. M, DNA size marker; Ext. DNA, extracted chromosomal DNA from *E. coli*.

to exert higher biocidal effects in US systems compared to Al_2O_3 particles [20]. To elucidate the difference between the effects of these two kinds of particles, a quantitative analysis was applied to determine the synergetic effect of TiO_2 in this process.

4.3. Quantitative analysis of DNA leaked by US/TiO_2 system

For quantitative comparison between the results obtained in the presence of TiO_2 and Al_2O_3 particles, the absorbance of leaked DNA in the irradiated solutions was determined at 260 nm. US irradiation in the presence of TiO_2 caused the leakage of more DNA into solution, indicating a higher cell lysis rate under these conditions. Also, leakage depended on time, and the absorbance of samples increased during the sonication period. However, these increases were leveled off after 15 min of irradiation; this is likely due to the termination of degradation of the leaked DNA in the solution.

US irradiation in the presence of Al_2O_3 also increased cell lysis and consequently promotes leakage. However, DNA leakage was significantly lower than in the solutions containing TiO_2. The study also compares the effects of these particles with those of blank samples without any particles. In the absence of any particles, the effect of US irradiation on cell lysis was negligible under these conditions.

4.4. Effects of radical scavenger on DNA release

The mechanism of cell lysis was further studied by investigating the effects of radical scavengers on the concentration of DNA leaked in the irradiated solutions. It has been reported that glutathione can inhibit the photodynamic DNA strand-breaking activity of TiO_2 [47]. The suppressing effects of this scavenger on *E. coli* inactivation were also reported in the previous paper [20]. Therefore, the effects of different concentrations of glutathione on the concentration of DNA leaked during US irradiation were studied. Glutathione was found to suppress the leakage of DNA during US irradiation, likely showing the suppression of cell lysis too. This suppressive effect was found to be concentration-dependent as well. Therefore, these results may indicate that OH radicals have a primary role in the degradation of DNA as well as cell lysis.

5. Possible mechanisms of enhanced OH radical formation and disinfection by US/TiO_2 system

The results reported herein indicate that the presence of TiO_2 accelerates OH radical formation and microbial inactivation during US irradiation even in the absence of UV irradiation. The results also lead us to propose the possible mechanisms for enhancement of OH radical formation and microbial inactivation by US/TiO_2 systems as illustrated in Fig. 1(B). The details are explained in the following sections.

5.1. Mechanisms of enhanced OH radical formation by US/TiO_2 system

The enhancement of OH radical formation by US/TiO_2 system may be mediated through the induction of cavitation bubbles in irradiating solutions, because the degassing of the irradiation solution completely blocked the formation of OH radicals in US/TiO_2 systems (Fig. 4). The presence of heterogeneous particles seems to increase the formation rate of cavitation bubbles by providing additional nuclei [44,50–53]. Cavitation increased due to the heterogeneous nucleation of bubbles would cause the induction of hot spots in the solution, resulting in the OH radical generation via pyrolysis of water. Although similar enhancements were obtained even in the presence of inert particles such as Al_2O_3, the oxidizing power obtained in the presence of TiO_2 was significantly higher than that obtained with Al_2O_3. This might be due to the OH radical generation via TiO_2 excitation under US irradiation, in addition to that via pyrolysis [48,49].

One possible reason for TiO_2 excitation under US irradiation might be very high temperatures (>5000 K) in the hot spots caused by cavitation bubble implosion, which can produce thermally excited positive holes on the TiO_2 surface. Mizuguchi et al. revealed the complete decomposition of polycarbonate mixed with TiO_2 when the mixture was heated to about 500 °C [54–56]. The mechanism was thought to be the successive decomposition of molten polycarbonate due to thermally excited positive holes at the TiO_2 surface. A large number of positive holes are expected to appear on the surface of high-temperature TiO_2. Nakajima et al. further demonstrated that the addition of TiO_2 was more effective than SiO_2 for the decomposition of 1,4-dioxane in water [57]. After examining the temperature change of water or TiO_2 suspension during sonication, they suggested that an endothermic process occurred in the TiO_2-added water, and that the thermal excitation of TiO_2 is the most plausible explanation of such a process.

Another possible reason for TiO_2 excitation under US irradiation might be the flushes of single-bubble sonoluminescence (SBSL) caused by bubble implosion. The SBSL involves intense UV light, which may induce the excitation of TiO_2 in the US system. Recent study indicated that the activation of TiO_2 photocatalyst by SBSL caused a significant decomposition of phenol and 2,4-dinitrophenol [58]. These observations may propose the possibility that US irradiation over a TiO_2 enhances the generation of OH radicals, and this effect is mediated by mechanisms similar to those of TiO_2 photocatalysis.

5.2. Mechanisms of enhanced disinfection rate by US/TiO_2 system

The improvement of disinfection rate by US/TiO_2 system may be attributed to the synergetic action of the enhancing the physical and chemical factor for cell inactivation, as shown in Fig. 1(B). With regard to the physical factor, the frequency of hot spot increased associating with the extreme high temperature and share stress, since cavitation bubble formation and implosion increased due to the addition of TiO_2, which serve as nuclei of cavitation bubble. For the chemical factor, generation of OH radical increased via both the sonocatalytic excitation of TiO_2 and the enhancing pyrolysis of water molecules by extreme temperature and sonoluminescence derived from cavitation bubble implosion, as descried in the foregoing section.

Based on the present and previous findings, we propose a more detailed mechanism for the bactericidal effect of the TiO_2 sonocatalytic reaction. The initial oxidative damage occurs on the cell wall, where the TiO_2 sonocatalytic surface makes first contact with intact cells. Cells with damaged walls are still viable. After the wall is no longer protected, oxidative damage occurs on the underlying cytoplasmic membrane. Sonocatalytic action progressively increases cell permeability and subsequently allows the free efflux of intracellular contents, leading eventually to cell death. Free OH radicals may also gain access to cells that have damaged membranes, and the subsequent direct attack on the intracellular components can accelerate cell death. Evidence for the molecular targets of attack in the cell envelope is the subject of an upcoming report from our laboratory, in which we demonstrate that lipid peroxidation can be initiated via a TiO_2 sonocatalytic reaction and may be an important cause of cell death. The OH radicals are primarily involved in this process.

Acknowledgments

This research was supported in part by Grants-in-Aid for Scientific Research (B) (no. 16310055 and no. 19300182, to N. Shimizu) from the Ministry of Education, Culture, Sports, Science, and Technology of Japan, and by the Industrial Technology Research Grant Program (no. 05A33020, to N. Shimizu and C. Ogino) in 2005 from the New Energy and Industrial Technology Development Organization (NEDO) of Japan.

References

[1] K.L. Simpson, K.P. Hayes, Water Res. 32 (1998) 1522–1528.
[2] J. Kuo, J. Chen, Water Environ. Res. 78 (2006) 1406–1428.
[3] S.W. Krasner, H.S. Weinberg, S.D. Richardson, S.J. Pastor, R. Chinn, M.J. Sclimenti, G.D. Onstad, A.D. Thruston Jr., Environ. Sci. Technol. 40 (2006) 7175–7185.
[4] J. Kuo, M. Kanada, Water Environ. Res. 79 (2007) 1474–1495.
[5] A. Adin, J. Katzhendler, D. Alkaslassy, C. Rav-Acha, Water Res. 25 (1991) 797–805.
[6] W.A. Mitch, D.L. Sedlak, Environ. Sci. Technol. 36 (2002) 588–595.
[7] G.D. Harris, V.D. Adams, D.L. Sorensen, K.R. Dupont, J. Water Pollut. Control Fed. 59 (1987) 781–787.
[8] J.A. Parker, J.L. Darby, Water Environ. Res. 67 (1995) 1065–1075.
[9] I. Hua, J.E. Thompson, Water Res. 34 (2000) 3888–3893.
[10] T.J. Mason, E. Joyce, S.S. Phull, J.P. Lorimer, Ultrason. Sonochem. 10 (2003) 319–323.
[11] M. Furuta, M. Yamaguchi, T. Tsukamoto, B. Yim, C.F. Stavarache, K. Hasiba, Y. Maeda, Ultrason. Sonochem. 11 (2004) 57–60.
[12] M. Kubo, R. Onodera, N. Shibasaki-Kitakawa, K. Tsumoto, T. Yonemoto, Biotechnol. Prog. 21 (2005) 897–901.
[13] P.R. Gogate, J. Environ. Manage. 85 (2007) 801–815.
[14] J.H. Gibson, D.H.N. Young, R.R. Farnood, P. Seto, Water Qual. Res. J. Can. 423 (2008) 23–35.
[15] S. Koda, M. Miyamoto, M. Toma, T. Matsuoka, M. Maebayashi, Ultrason. Sonochem. 16 (2009) 655–659.
[16] I. Oyane, T. Takeda, Y. Oda, T. Sakata, M. Furuta, K. Okitsu, Y. Maeda, R. Nishimura, Ultrason. Sonochem. 16 (2009) 532–536.
[17] T.D. Yuri, B.Mc. William, K.S. Suslick, J. Am. Chem. Soc. 121 (1999) 5817–5818.
[18] K.S. Suslick, Homogeneous sonochemistry, in: K.S. Suslick (Ed.), Ultrasound: Its Chemical, Physical and Biological Effects, VHC, New York, 1988, pp. 123–163.
[19] R.E. Verrall, C.M. Sehgal, Sonoluminescence, in: K.S. Suslick (Ed.), Ultrasound: Its Chemical, Physical and Biological Effects, VHC, New York, 1988, pp. 227–286.
[20] M.F. Dadjour, C. Ogino, S. Matsumura, N. Shimizu, Biochem. Eng. J. 25 (2005) 243–248.
[21] M.F. Dadjour, C. Ogino, S. Matsumura, S. Nakamura, N. Shimizu, Water Res. 40 (2006) 1137–1142.
[22] C. Ogino, M.F. Dadjour, K. Takaki, N. Shimizu, Biochem. Eng. J. 32 (2006) 100–105.
[23] P.-C. Maness, S. Smolinski, D.M. Blake, Z. Huang, E.J. Wolfrum, W.A. Jacoby, Appl. Environ. Microbiol. 65 (1999) 4094–4098.
[24] A.B. Pandit, P.R. Gogate, S. Mujumdar, Ultrason. Sonochem. 8 (2001) 227–231.
[25] M. Kubo, K. Matsuoka, A. Takahashi, N. Shibasaki-Kitakawa, T. Yonemoto, Ultrason. Sonochem. 12 (2005) 263–269.

[26] J. Wang, B. Guo, X. Zhang, Z. Zhang, J. Han, J. Wu, Ultrason. Sonochem. 12 (2005) 331–337.
[27] A. Fujishima, T.N. Rao, D.A. Tryk, J. Photochem. Photobiol. C: Photochem. Rev. 1 (2000) 1–21.
[28] B.N. Lee, W.D. Liaw, J.C. Lou, Environ. Eng. Sci. 16 (1999) 165–175.
[29] J.A. Herrera Melian, J.M. Dona Rodriguez, A. Viera Suarez, E. Tello Rendon, C. Valdes do Campo, J. Arana, J. Perez Pena, Chemosphere 41 (2000) 323–327.
[30] S. Yamazaki, S. Matsunaga, K. Hori, Water Res. 35 (2001) 1022–1028.
[31] T. Sato, M. Taya, Biochem. Eng. J. 28 (2006) 303–308.
[32] M. Grootveld, B. Halliwell, Biochem. J. 237 (1986) 499–504.
[33] L. Diez, M.H. Livertoux, A.A. Stark, M. Wellman-Rousseau, P. Leroy, J. Chromatogr. B 763 (2001) 185–193.
[34] C.B. Amphlett, G.E. Adams, B.D. Michael, Adv. Chem. Ser. 81 (1968) 231–250.
[35] N. Shimizu, C. Ogino, M.F. Dadjour, K. Ninomiya, A. Fujihira, K. Sakiyama, Ultrason. Sonochem. 15 (2008) 988–994.
[36] M.K. Eberhardt, R. Colina, J. Org. Chem. 53 (1988) 1071–1074.
[37] A. Henglein, C. Kormann, Int. J. Radiat. Biol. 48 (1985) 251–258.
[38] S. Goldstein, G. Czapski, Int. J. Radiat. Biol. 46 (1984) 725–729.
[39] H.G. Flynn, Physics of acoustic cavitation in liquids, in: W.P. Mason (Ed.), Physical Acoustics. Principles and Methods, Vol. 1, Part B, Academic Press, New York, 1964, pp. 58–172.
[40] I.Z. Shirgaonkar, A.B. Pandit, Ultrason. Sonochem. 5 (1998) 53–61.
[41] Y. Suzuki, A. Maezawa, S. Uchida, Jpn. J. Appl. Phys. 39 (2000) 2958–2961.
[42] L. Davydov, E.P. Reddy, P. France, P.G. Smirniotis, Appl. Catal. B 32 (2001) 95–105.
[43] M. Mrowetz, C. Pirola, E. Selli, Ultrason. Sonochem. 10 (2003) 247–254.
[44] N.H. Ince, R. Belen, Environ. Sci. Technol. 35 (2001) 1885–1888.
[45] N. Shimizu, C. Ogino, M.F. Dadjour, T. Murata, Ultrason. Sonochem. 14 (2007) 184–190.
[46] T. Ashikaga, M. Wada, H. Kobayashi, M. Mori, Y. Katsumura, H. Fukui, S. Kato, M. Yamaguchi, T. Takamatsu, Mutat. Res. 466 (2000) 1–7.
[47] C.B. Pocernich, M. La Fontaine, D.A. Butterfield, Neurochem. Int. 36 (2000) 185–191.
[48] M.P. Brenner, S. Hilgenfeldt, D. Lohse, Rev. Mod. Phys. 74 (2002) 425–484.
[49] C. Ogino, M.F. Dadjour, Y. Iida, N. Shimizu, J. Hazard. Mater. 153 (2008) 551–556.
[50] H. Sekiguchi, Y. Saita, J. Chem. Eng. Jpn. 34 (2001) 1045–1048.
[51] H.B. Marschall, K.A. Mørch, A.P. Keller, M. Kjeldsen, Phys. Fluids 15 (2003) 545–553.
[52] T. Tuziuti, K. Yasui, Y. Iida, H. Taoda, S. Koda, Ultrasonics 42 (2004) 597–601.
[53] T. Tuziuti, K. Yasui, M. Sivakumar, Y. Iida, N. Miyoshi, J. Phys. Chem. A 109 (2005) 4869–4872.
[54] J. Mizuguchi, T. Shinbara, J. Appl. Phys. 96 (2004) 3514–3519.
[55] T. Shinbara, T. Makino, K. Matsumoto, J. Mizuguchi, J. Appl. Phys. 98 (2005), 044909 1-5.
[56] K. Matsumoto, T. Makino, T. Ebara, J. Mizuguchi, J. Chem. Eng. Jpn. 41 (2008) 51–56.
[57] A. Nakajima, H. Sasaki, Y. Kameshima, K. Okada, H. Harada, Ultrason. Sonochem. 14 (2007) 197–200.
[58] H. Ogi, M. Hirao, M. Shimoyama, Ultrasonics 40 (2002) 649–650.

Bioorganic & Medicinal Chemistry Letters 20 (2010) 5320–5325

Contents lists available at ScienceDirect

Bioorganic & Medicinal Chemistry Letters

journal homepage: www.elsevier.com/locate/bmcl

Construction of protein-modified TiO_2 nanoparticles for use with ultrasound irradiation in a novel cell injuring method

Chiaki Ogino [a,b], Naonori Shibata [a], Ryosuke Sasai [a], Keiko Takaki [b], Yusuke Miyachi [a,d], Shun-ichi Kuroda [c], Kazuaki Ninomiya [b], Nobuaki Shimizu [a,b,*]

[a] The Division of Material Sciences, Graduate School of Neutral Science and Technology, Kanazawa University, Kakuma, Kanazawa 920 1192, Japan
[b] Institute of Nature and Environmental Technology, Kanazawa University, Kakuma, Kanazawa 920 1192, Japan
[c] Department of Structural Molecular Biology, The Institute of Scientific and Industrial Research (ISIR), Osaka University, Mihogaoka 8-1, Ibaraki, Osaka 567 0047, Japan
[d] Department of Chemical Science and Engineering, Graduate School of Engineering, Kobe University, Rokkoudaichou, Nada-ku, Kobe 657 8501, Japan

ARTICLE INFO

Article history:
Received 26 March 2010
Revised 21 June 2010
Accepted 23 June 2010
Available online 1 July 2010

Keywords:
TiO_2 nanoparticle
Hepatitis B virus
Drug delivery system
Ultrasound irradiation
OH radical

ABSTRACT

Recently, our group discovered an alternative titanium dioxide (TiO_2) activation method that uses ultrasound irradiation (US/TiO_2) instead of ultraviolet irradiation. The pre-S1/S2 protein from hepatitis B virus, which recognizes liver cells, was immobilized to the surface of TiO_2 nanoparticles using an amino-coupling method. The ability of the protein-modified TiO_2 nanoparticles to recognize liver cells was confirmed by surface plasmon resonance analysis and immuno-staining analyses. After uptake of TiO_2 nanoparticles by HepG2 cancer cells, the cells were injured using this US/TiO_2 method; significant cell injury was observed at an ultrasound irradiation intensity of 0.4 W/cm^2. Together with these results, this strategy could be applied to new cell injuring systems that use ultrasound irradiation in place of photodynamic therapy in the near future.

Titanium dioxide (TiO_2) is a photocatalyst and reactive oxygen species (ROS) can be generated on the surface of TiO_2 by ultraviolet irradiation (λ <390 nm).[1,2] Because ROS strongly catalyze reactions that result in degradation of many harmful chemicals, the killing of microorganisms,[3,4] and injury of mammalian cells,[5,6] TiO_2 has been used as a photocatalyst in sanitization processes to maintain clean environments in hospitals.[7] Recently, our group discovered an alternative TiO_2-activation method that uses ultrasound irradiation (US/TiO_2) instead of ultraviolet irradiation.[8] The US/TiO_2 method produced an OH radical upon combination with methylene blue—a typical substrate for photocatalytic reactions—and other various radical scavengers. Although ultrasound irradiation in aqueous media is known to produce various ROS, including OH radicals and superoxide anion oxygen radicals (O_2^-), it was assumed that production of ROS, including OH radicals, was enhanced using the US/TiO_2 method. Furthermore, production of ROS using the US/TiO_2 method with pellet-type TiO_2, such as ceramics, had been previously applied to chemical degradation[8–10] and to killing microorganisms such as an *Escherichia coli*[11,13] and *Legionella* strains.[12] The advantage of the US/TiO_2 method over the typical photo-excitation and ultraviolet irradiation methods is that it can be used on non-transparent media. Because sound waves generated by ultrasound can transmit through non-transparent media, TiO_2 located within non-transparent media, such as the human body, can be activated by ultrasound, but not by photo-excitation or ultraviolet radiation.

Photodynamic therapy (PDT) is well-known as a novel approach to cancer treatment based on the produced ROS. Typical PDT is carried out using the combination of a photosynthesizer, such as porphyrin IX, and an activator, typically a laser. PDT works by producing ROS that result in cell injury or death. However, the application of PDT is limited to the laser-irradiated area, so the clinical use of PDT has been restricted to cases of skin cancer.[14,15]

Because the ROS generated on the surface of TiO_2 have very short half-lives,[16] a large portion of the ROS disappear during diffusion in aqueous media without participating in any cell injuring or killing. Therefore, delivery of TiO_2 nanoparticles to specific target tissues is required for effective cell injuring using the US/TiO_2 method. However, TiO_2 has no cell-recognition potential. Moreover, the OH residues on the surface of TiO_2 nanoparticles easily associate with each other at neutral pH, resulting in aggregation of nanoparticles.[17] After aggregation occurs, the nanoparticles are no longer able to transfer into blood and therefore have no adaptation to clinical utility. Sonezaki et al. constructed TiO_2 nanoparticles that remained in suspension at neutral pH by surface modification of the nanoparticles with polyacrylic acid (PAA) at high temperature.[18] Because the dissociation constant of the carboxylic acid group of PAA is approximately $pK_a = 4.0$,[19] the carboxylic acid group of PAA can dissociate

* Corresponding author. Tel.: +81 76 234 4807; fax: +81 76 234 4829.
E-mail address: nshimizu@t.kanazawa-u.ac.jp (N. Shimizu).

0960-894X/$ - see front matter © 2010 Elsevier Ltd. All rights reserved.
doi:10.1016/j.bmcl.2010.06.124

into anionic ion in neutral pH solution, and these electric charge assist of stable formation of TiO_2 nanoparticle. In addition, the carboxylic acid group of PAA allows an immobilization of proteins to the nanoparticles via covalent bond with amino groups.

Therefore, based on the concept of ROS utilization in cancer therapy, in sanitation, and in methods of modifying TiO_2 nanoparticles, the purpose of the present study was to apply the US/TiO_2 method to mammalian cell killing or injuring via ROS production. To achieve this goal, the ability of protein-modified TiO_2 nanoparticles targeted to specific tissues was investigated. In particular, the pre-S1/S2 protein, which is part of the L protein from hepatitis B virus[20] and recognizes hepatocytes, was immobilized on the surface of TiO_2 nanoparticles. Subsequently, the ability of the protein-modified TiO_2 nanoparticles to produce OH radicals was investigated.

Escherichia coli BL21(DE3) (Merck KGaA Novagen, Darmstadt, Germany) was used for the recombinant protein expression. The plasmids, pGEX-GFP-pre-S1/S2 and pGEX-GFP,[21] were used for production of the fusion recombinant proteins, GST-GFP-pre-S1/S2 and GST-GFP, respectively. Using the production of GST-GFP-pre-S1/S2 as an example, a single colony of the transformant, harboring the pGEX-GFP-pre-S1/S2 plasmid, was inoculated into a test tube containing 3 ml of LB medium [1% (w/v) tryptone, 0.5% (w/v) yeast extract and 0.5% (w/v) NaCl] supplemented with 100 μg/ml ampicillin and incubated at 37 °C for 8 h with shaking (200 rpm). The culture medium (1 ml) was then seeded into a flask containing 200 ml LB medium with 100 μg/ml ampicillin, and incubated at 37 °C for approximately 3 h. When the absorbance at 600 nm of the culture medium reached 1.0 by spectrophotomer (U-3000, Hitachi, Tokyo, Japan), the cultivation temperature was decreased to 17 °C and IPTG was added to the culture medium at a final concentration of 0.1 mM for inducing of recombinant protein production. After 12 h of incubation, the cells were collected by centrifugation at 10,000g for 10 min, rinsed twice with running buffer (20 mM Hepes buffer (pH 8.0)), and suspended in 30 ml of running buffer containing 100 μg/ml PMSF as a protease inhibitor. The cytoplasmic fraction was extracted by ultrasonication on ice for 5 min (output = 100 W, duty = 40%, frequency = 20 kHz), and the supernatant was collected by centrifugation at 10,000g for 10 min. The pellet containing the inclusion body fraction was washed twice with 10 ml of wash buffer (20 mM Hepes, 0.5% (v/v) Triton X-100, and 1 mM EDTA, pH 8.0), re-suspended with folding buffer (20 mM Hepes, 1 mM DTT, and 1 mM EDTA) containing 8 M urea, and incubated at room temperature for 1 h. After centrifugation, the supernatant containing the denatured recombinant protein was dialyzed with folding buffer containing 4 M urea for 3 h at 4 °C. Subsequently, the supernatant was dialyzed with folding buffer containing 2 M urea for 3 h at 4 °C, and then dialyzed with folding buffer overnight at 4 °C. The sample then was centrifuged at 10,000g for 10 min, and the supernatant containing the recombinant GST-GFP-pre-S1/S2 protein was immobilized on PAA-TiO_2 nanoparticles as follow: Polyacrylic acid-modified TiO_2 particles (PAA-TiO_2, average diameter of 102 nm) were constructed as previously described[18] using a MPT-422 TiO_2 suspension (Ishihara Sangyo Kaisha, Ltd, Osaka, Japan) as the starting material. GST-GFP-pre-S1/S2 and GST-GFP were immobilized onto the surface of the TiO_2 nanoparticles by chemical coupling at the carboxyl residue. The PAA-TiO_2 suspension (1.5% (w/v), 2.5 ml) was gently mixed with 0.5 ml of activating solution (0.2 M 1-ethyl-3(3-dimethyl-aminopropyl)carbodiimide hydrochloride (ECD) and 0.05 M *N*-hydroxy succinimide (NHS)), and the mixture was incubated at room temperature for 1 h. Then, the PAA-TiO_2 suspension was applied to a PD-10 column (GE Healthcare Bio-Science AB, Uppsala, Sweden) to exchange the buffer solution for 20 mM HEPES buffer (pH 8.0), and remove un-reacted ECD and NHS. An eluted sample (3.5 ml) of the activated PAA-TiO_2 suspension was mixed with 2.5 ml of the recombinant protein solution (approximately 1–2 mg/ml), and the mixture was incubated at 4 °C overnight. Subsequently, 1.0 ml of 0.1 M ethanolamine solution was added to block activated carboxyl residues and the mixture was incubated at 4 °C for an additional 30 min. The reacted mixture was separated using size exclusion chromatograph equipped with a AKTA FPLC (GE Healthcare Bio-Science AB, Uppsala, Sweden). In detail, 2.0 ml of sample was subjected to a Sephacryl S-500 HR column (16 × 300 mm, total bed volume 64 ml (GE Healthcare Bio-Science AB, Uppsala, Sweden)) that had been pre-equilibrated with 20 mM HEPES buffer (pH 7.4). Elution was performed with 0.5 ml/ml, and a sample was collected every 8 min (4 ml/tube). The size distribution of the protein-modified TiO_2 nanoparticles in each fraction was measured using a high performance particle sizer (HPP5001, Sysmex, Kobe, Japan). Immobilization of the recombinant protein on the TiO_2 nanoparticles was confirmed by surface plasmon resonance (SPR) analysis and sodium dodecyl sulphate polyacrylamide gel electrophoresis (SDS–PAGE). The weight of the TiO_2 particles was determined by the difference in particle weight before and after drying at 650 °C for 30 min. SPR analysis of the protein-modified TiO_2 nanoparticles was carried out using a BIACORE2000 (Biacore Life Sciences, Uppsala, Sweden). Anti-pre-S1 protein (80 μl) monoclonal antibody (0.5 mg/ml, Institute of Immunology Co., Ltd, Tokyo, Japan) was immobilized onto the CM-5 chip by chemical coupling with EDC and NHS according to the manufacturer's instruction manual. The interaction between GST-GFP-pre-S1/S2 protein-modified TiO_2 nanoparticles and the antibody was analyzed. The interactions of BSA-modified and unmodified TiO_2 nanoparticles with the antibody also were analyzed. In addition, for topographic observation of TiO_2 nanoparticles using atomic force microscopy (AFM), 10 μl of GST-GFP-pre-S1/S2 protein-modified TiO_2 nanoparticle suspension (0.002 (%) (w/v)) was dropped onto a cover glass (Matsunami, Japan) and dried under an air atmosphere. The topographic observation and average particle size analysis were performed using the dynamic force mode of AFM (SPA400 equipped with Nanonavi computer station, SIINT, Tokyo, Japan) with SI-DF20 as a cantilever.

Recombinant GST-GFP-pre-S1/S2 protein was recovered from the inclusion body fraction of cultivated transformant *E. coli* and refolded to form the soluble protein by dialyzing with folding buffers containing graded concentrations of urea (8 M to 0 M). The recovered sample was confirmed to be a single protein, approximately 72 kDa in size, by SDS–PAGE analysis (data not shown), and the purified protein concentration was estimated to be 2.98 mg/ml using the Bradford method. The GST-GFP-pre-S1/S2 protein was immobilized on the surface of the TiO_2 nanoparticles (average diameter 102 nm, see Table 1) by chemical coupling between the terminal amino group of the protein and the terminal carboxyl group of polyacrylic acid. The protein-modified TiO_2 nanoparticles were purified by size exclusion chromatography. The protein-modified TiO_2 nanoparticle suspended in 20 mM HEPES buffer was eluted in the void fraction and was completely separated from the unbound free protein (data not shown). The protein-modified TiO_2 nanoparticle suspension was stable in culture medium for at least 2 days (Table 1), although there was slight

Table 1
Average particle size of GST-GFP-pre-S1/S2-modified TiO_2 nanoparticles

Particle type	Average size (nm)
PAA-TiO_2	102
GST-GFP-pre-S1/S2 immobilized TiO_2 (immediately)	120[a]
GST-GFP-pre-S1/S2 immobilized TiO_2 (after 1 day)	136[a]
GST-GFP-pre-S1/S2 immobilized TiO_2 (after 2 days)	174[a]

[a] The particle size distribution analysis was performed after re-suspension in DMEM.

particle aggregation after static incubation at 4 °C. Furthermore, AFM analysis of GST-GFP-pre-S1/S2-modified TiO_2 nanoparticles showed protein-modified TiO_2 nanoparticles were of similar diameter (Fig. 1), and the average particle size based on topographic measurements was estimated to be 152 nm (data not shown). Each evaluation result was well agreed, and strongly indicated that the protein-modified TiO_2 nanoparticle form 100 to 150 nm scale size nanoparticle without particle aggregation. The molecular interaction between the anti-preS1 antibody and the protein-modified TiO_2 nanoparticles was investigated using a SPR sensor. First, a solution of free GST-GFP-pre-S1/S2 protein was applied to a CM-5 chip coated with anti-pre-S1 antibody equipped with BIACORE2000 (Fig. 2A). The resonance unit was increased in a dose-dependent manner and the antibody immobilized on the chip recognized pre-S1 protein. Next, GST-GFP-pre-S1/S2-modified TiO_2 nanoparticles were applied to the same chip (Fig. 2B). Although the immobilized protein concentration of the TiO_2 nanoparticle suspension was 0.8 μM, a significant interaction was observed. As a control, TiO_2 nanoparticles were modified with the same concentration of bovine serum albumin (BSA); there was no significant increase in the resonance unit. Therefore, it was concluded that the GST-GFP-pre-S1/S2 protein was covalently bound by chemical coupling to the surface of the TiO_2 nanoparticles without any denaturation of the protein.

Human hepatoma HepG2 cells were cultured in Dulbecco's modified Eagle medium (DMEM, Nakarai Tesqu, Kyoto, Japan), supplemented with 10% (v/v) fetal bovine serum (FBS; Invitrogen GIBCO, Carlsbad, CA, USA), 60 μg/ml penicillin (Nakarai Tesqu, Kyoto, Japan), and 100 μg/ml streptomycin (Nakarai Tesqu, Kyoto, Japan). The cells were maintained at 37 °C and under a 5% CO_2 atmosphere. Approximately 2×10^5 HepG2 cells, counted by hematometer, suspended in 2 ml DMEM were seeded in 35-mm culture dishes and incubated for 24 h. Then, the recombinant protein-modified TiO_2 nanoparticles suspension were added to the culture medium at a final concentration of 0.01% (w/v) (=0.1 g/l) of TiO_2 and cultured for an additional 6 h because it was reported about the complete uptake of BNC was attained within 6 h in HepG2.[20] After additional cultivation, the culture dishes were washed twice with 500 μl of PBS(−) buffer. To immobilize the cells, 500 μl paraformaldehyde (PFA) solution (4%) was added to the dish, followed by incubation at room temperature for 15 min. After removal of the PFA solution, cells were permeabilized with 500 μl of 0.25% (w/v) Triton X-100 in PBS(−) buffer for 15 min. Then, the primary antibody solution (500 μl of 1 μg/ml anti-pre-S1 or 4.4 μg/ml anti-GFP monoclonal antibody (Nakarai Tesqu, Kyoto, Japan)) in PBS(−) buffer was added to the dish, followed by an overnight incubation at 4 °C. After washing three times with 0.03% (w/v) Triton X-100 in PBS(−) buffer, the secondary antibody solution (500 μl, 4 μg/ml Alexa Fluor 555 goat anti-mouse IgG antibody (Invitrogen, Carlsbad, CA, USA)) was added to the dish, followed by incubation at room temperature for 1 h. After washing three times with 0.03% (w/v) Triton X-100 in PBS(−) buffer, uptake of protein-modified TiO_2 nanoparticles by HepG2 cells was observed using a fluorescent microscope (BZ-8000, KEYENCE, Osaka, Japan). After incubation of HepG2 cells with protein-modified TiO_2 nanoparticles for 6 h, the uptake of TiO_2 nanoparticles was observed by fluorescent microscopy (Fig. 3). Cell morphology was unchanged by incubation with TiO_2 nanoparticles (Fig. 3A, C, G, and I) or with free protein (Fig. 3B and H). Free GST-GFP-pre-S1/S2 protein recognized HepG2 cells, and its clearance was nearly complete after a 6-h incubation period (Fig. 3E and K). The uptake of GST-GFP-pre-S1/S2-modified TiO_2 nanoparticles also was observed by staining with anti-preS1 and anti-GFP monoclonal antibodies (Fig. 3D and J). The fluorescence signal was observed proximal to the cell membrane. The GST-GFP-pre-S1/S2-modified TiO_2 nanoparticles appeared to adhere to the cell membrane, but did not translocate into the cytosol fraction. As a negative control, the uptake of GST-GFP-modified TiO_2 nanoparticles also was investigated (Fig. 3F and L); there was no evidence of GST-GFP-modified TiO_2 nanoparticle uptake. In addition, there was no evidence of non-specific endocytosis of TiO_2 nanoparticles by HepG2 cells (Fig. 3L). Based on these observations, it was assumed that the GST-GFP-pre-S1/S2-modified TiO_2 nanoparticles specifically recognized the HepG2 cells.

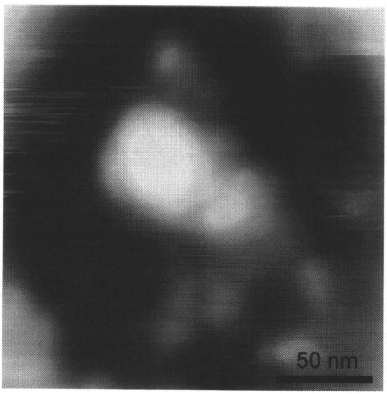

Figure 1. Topographic observation of GST-GFP-pre-S1/S2-modified TiO_2 nanoparticles using AFM. Scale bar indicates 50 nm.

Aminophenyl fluorescein (APF, Daiichi Pure Chemicals Co., Ltd, Tokyo, Japan) was used to quantify OH radicals. The APF solution (1 μM) was prepared with PBS(−) buffer. APF solution (2 ml) was added to each dish, and subsequently, protein-modified TiO_2 nanoparticles were added at a final concentration of 0.01% (w/v). Then, each dish was irradiated with high frequency ultrasound (1 MHz) at intensity varied between 0 and 2.0 (W/cm^2) for 30 s. The amount of fluorescein generated from the reaction of APF with OH radicals was measured using a multi-well plate reader CytoFluor 4000 (Applied Biosystems, Foster City, CA, USA) at an excitation wavelength of 490 nm and an emission wavelength of 515 nm. OH radical generation from both rutile and anatase TiO_2 particles using ultrasound irradiation has been confirmed.[8] This method has been established for killing of various microorganisms, such as *E. coli* and *Legionella*.[11–13] Based on these previous findings and on the targeting potential of protein-modified TiO_2 nanoparticles, effective cell injuring using the combination of ultrasound irradiation and TiO_2 nanoparticles was investigated. First, the OH radical generation ability of TiO_2 nanoparticles in the absence of cultured cells was measured by high frequency ultrasound irradiation (1 MHz) (Fig. 4). Although ultrasound irradiation itself has OH radical-generating potential, the additional PAA-TiO_2 nanoparticles enhanced OH radical production 1.3–1.5-fold at intensity of 0.4 W/cm^2. In addition, the capacity of protein-modified TiO_2 nanoparticles to generate OH radicals exhibited the same response (data not shown). Therefore, it was assumed that PAA-TiO_2 nanoparticles had the potential to generate OH radicals.

For evaluating of cell injury resulting from the combination of TiO_2 nanoparticles and ultrasound irradiation, after incorporating protein-modified TiO_2 nanoparticles, HepG2 cells were washed three times with fresh DMEM (2 ml) and were then re-suspended in 2 ml DMEM. Ultrasound irradiation was performed as follows:

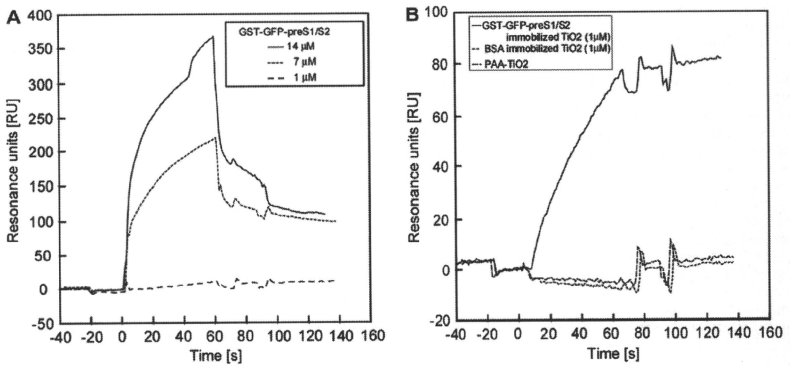

Figure 2. Confirmation of GST-GFP-pre-S1/S2 immobilization on the surface of TiO_2 nanoparticles. The sensorgram of free GST-GFP-pre-S1/S2 (A) and GST-GFP-pre-S1/S2-modified TiO_2 nanoparticles (B) using anti-preS1 antibody was analyzed using BIACORE2000.

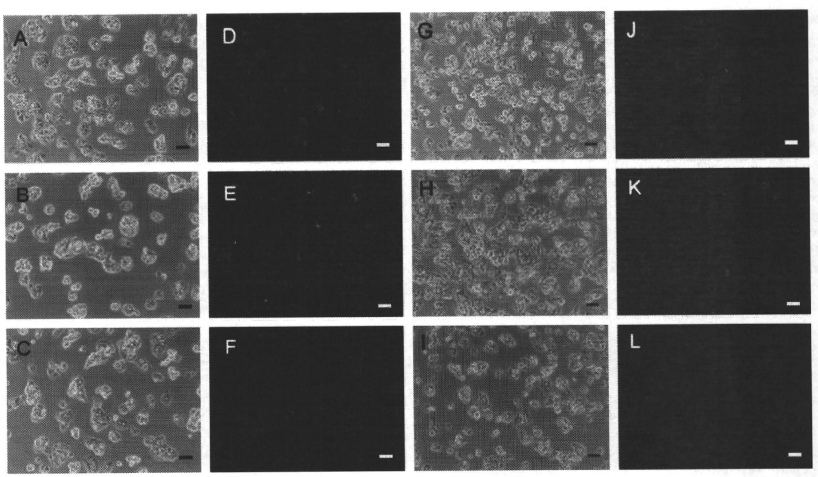

Figure 3. Immuno-staining of HepG2 for uptake of GST-GFP-pre-S1/S2-modified TiO_2 nanoparticles. The uptake of GST-GFP-prs-S1/S2-modified TiO_2 nanoparticles (A, D, G, J), free GST-GFP-pre-S1/S2 protein (B, E, H, K) and GST-GFP-modified TiO_2 nanoparticles (C, F, I, L) was confirmed by fluorescent microscopy after staining with anti-preS1 monoclonal antibody (A–F) and anti-GFP monoclonal antibody (G–L), respectively. Phase-contrast images are shown in panels A–C and G–I and fluorescent images are presented in panels D–F and J–L. Each scale bar indicates 50 μm.

frequency, 1 MHz; duty, 50%; and, irradiation time, 30 s. After irradiation, lactose dehydrogenase (LDH) activity leaked from damaged cells into the culture medium was measured using a CytoTox-One homogeneous membrane integrity assay kit (Promega, Madison, WIS, USA). In brief, the fluorescence intensity of the final product, resorufin, which is produced by a sequential reaction involving LDH, was measured using a multi-well plate reader, CytoFluor 4000, at an excitation wavelength of 560 nm and an emission wavelength of 590 nm. Cell-injury was performed using the US/TiO_2 method and cell damage was monitored by measuring the amount of LDH that leaked out of the cell (Fig. 5). At 0.6 W/cm^2, the fluorescent intensities, which were indicative of leaked LDH, were saturated in each experimental condition; therefore, it was assumed that most cells were killed. In contrast, there were no significant differences among the three conditions at intensity of 0.2 W/cm^2. Therefore, this irradiation intensity was deemed insufficient for significant cell injury, as OH radicals were not generated under this condition (Fig. 4). At an irradiation intensity of 0.4 W/cm^2, LDH leakage was subsequently increased by addition of TiO_2 nanoparticles, and LDH activity was saturated in the

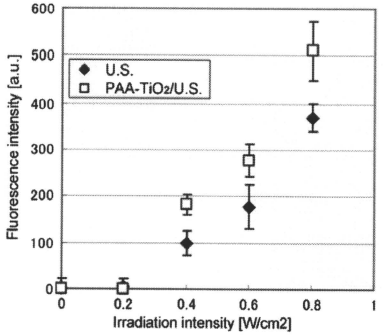

Figure 4. Measurement of OH radical generation by modified TiO_2 nanoparticles as a result of high frequency ultrasound irradiation. Generation of OH radicals was measured using ultrasonic irradiation with PAA-TiO_2 (open box) and without any particle (close diamond). Data are the mean of six independent experiments, and the error bar indicates the standard deviation.

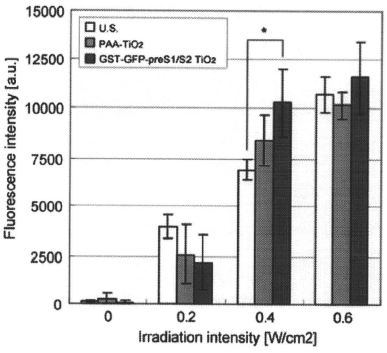

Figure 5. Membrane injury in HepG2 cells as a result of the combination of TiO_2 nanoparticles and ultrasound irradiation. LDH leaked from cells as a result of membrane injury was measured. Data are the mean of seven independent experiments, and the error bar indicates the standard error. Significant difference between groups (p <0.05, one-way ANOVA).

presence of GST-GFP-pre-S1/S2-modified TiO_2 nanoparticles. Based on these results, it was assumed that TiO_2 nanoparticles localized to HepG2 cells as a result of the pre-S1/S2 protein-enhanced OH radical generation, thereby injuring the cells.

The PAA-TiO_2 nanoparticles were approximately 100 nm in diameter; protein-modification increased particle diameter (Table 1). The increment in diameter was 20 nm, and it was assumed that the increased length was equivalent to the sum of the diameters of two protein molecules, as immobilized protein covered the TiO_2 nanoparticles in a single layer. Based on the theory of Flory, the diameter of GST-GFP-pre-S1/S2 was estimated to be 7 nm;[22] therefore, the increased diameter of the nanoparticles was consistent with this theoretical estimate. The number of protein molecules immobilized on each TiO_2 nanoparticle was estimated to be 420 using the following parameters: average diameter of each TiO_2 nanoparticle, 100 nm; protein concentration of GST-GFP-pre-S1/S2, 64 mg/L; TiO_2 nanoparticle concentration, 3 g/L; specific gravity of TiO_2 nanoparticles, 4.5 g/cm^3; and, the putative globule diameter of GST-GFP-pre-S1/S2 protein, 10 nm. The theoretical values for these parameters were as follows: number of protein molecules per nanoparticle, approximately 440; putative globule protein diameter, 10 nm; and, nanoparticle diameter, 100 nm. Applying these theoretical values to TiO_2 nanoparticles covered with a single layer of protein molecules, there was good agreement between the measured and theoretical number of protein molecules per nanoparticle. The theoretical estimates suggest that the surface of TiO_2 nanoparticles was completely covered with protein molecules.

The GST-GFP-pre-S1/S2 protein displayed on the surface of the TiO_2 nanoparticles was recognized by the anti-preS1 antibody (Fig. 2B), and allowed the nanoparticles to be localized to the HepG2 cells (Fig. 3D and J). Moreover, the protein-modified TiO_2 nanoparticles were capable of OH radical generation even though the particle surface was covered with protein (Fig. 4). Based on these results, it was concluded that the protein-modified TiO_2 nanoparticles have a dual function: targeting TiO_2 nanoparticles to specific cells and generating OH radicals that result in cell injury. The GST-GFP-pre-S1/S2-modified TiO_2 nanoparticles were localized in the vicinity of the cell membrane (Fig. 3D and J), while the free GST-GFP-pre-S1/S2 protein translocated to the cytosol (Fig. 3E and K). Although the fusion between hepatitis B virus and liver cells was complete after 6 h in a previous study,[20] only partial fusion occurred between the nanoparticles and HepG2 cells in this study. Therefore, it was assumed that the protein-modified nanoparticles cannot be cleared by endocytosis.

Ultrasound irradiation at intensity of 0.4 W/cm^2 and a frequency of 1 MHz to HepG2 cells that had incorporated TiO_2 nanoparticles resulted in cell damage (Fig. 5). The number of OH radicals generated in the presence of TiO_2 nanoparticles at 0.4 W/cm^2 was equivalent to that at 0.6 W/cm^2 in the absence of TiO_2 nanoparticles (Fig. 4). Therefore, it was assumed that cell damage could be induced by these OH radical concentrations, regardless of the experimental conditions. Because the high ultrasound irradiation intensity could be damage to the TiO2 non-delivered cell, a comparable lower intensity should be required for target cell damaged irradiation. There are several possible ways to improve cell damage efficiency at lower ultrasound irradiation intensity as follows: enhance the immobilization efficiency of GST-GFP-pre-S1/S2 protein to the TiO_2 nanoparticles; improve, either directly or indirectly, the ultrasound irradiation method; and change the frequency of ultrasound irradiation. Furthermore, the combination of ultrasound and ultraviolet irradiation could be gain an advanced improvement of irradiation efficiency. In addition, the mechanism of cell injury that occurs as a result of the US/TiO_2 method warrants investigation, as it has not been studied.

As a conclusion, this is the first study demonstrating the use of TiO_2 nanoparticles to cause cell-specific damage. The protein-modification in the TiO_2 nanoparticles served the dual functions of specific cell-recognition and OH radical generation. Modification of TiO_2 nanoparticles with various targeting proteins, such antibodies or epidermal growth factor (EGF), will allow this method to be used to target specific cancer cells. Furthermore, the combination of ultrasound irradiation and TiO_2 nanoparticle will be an alternative targeted tissue specific cancer cell treatment methodology such like a PDT in the near future.

Acknowledgments

This work was supported, in part, by a Grant-in-aid from the Ministry of Education, Culture, Sports, Science and Technology, Japan (Nos. 18650143 and 18015019 to N.S.).